Determination of the optical properties of $La_{2-x}Ba_xCuO_4$ for several dopings, including the anomalous $x = \frac{1}{8}$ phase

C. C. Homes,* M. Hücker, Q. Li, Z. J. Xu, J. S. Wen, G. D. Gu, and J. M. Tranquada
Condensed Matter Physics and Materials Science Department, Brookhaven National Laboratory, Upton, New York 11973, USA
(Received 17 October 2011; revised manuscript received 22 March 2012; published 11 April 2012)

The optical properties of single crystals of the high-temperature superconductor $La_{2-x}Ba_xCuO_4$ have been measured over a wide frequency and temperature range for light polarized in the *a-b* planes and along the *c* axis. Three different Ba concentrations have been examined, $x = 0.095$ with a critical temperature $T_c = 32$ K, $x = 0.125$ where the superconductivity is dramatically weakened with $T_c \simeq 2.4$ K, and $x = 0.145$ with $T_c \simeq 24$ K. The in-plane behavior of the optical conductivity for these materials at high temperature is described by a Drude-like response with a scattering rate that decreases with temperature. Below T_c in the $x = 0.095$ and 0.145 materials there is a clear signature of the formation of a superconducting state in the optical properties allowing the superfluid density (ρ_{s0}) and the penetration depth to be determined. In the anomalous 1/8 phase, some spectral weight shifts from lower to higher frequency ($\gtrsim$300 cm^{-1}) on cooling below the spin-ordering temperature $T_{so} \simeq 42$ K, associated with the onset of spin-stripe order; we discuss alternative interpretations in terms of a conventional density-wave gap versus the response to pair-density-wave superconductivity. The two dopings for which a superconducting response is observed both fall on the universal scaling line $\rho_{s0}/8 \simeq 4.4\sigma_{dc}T_c$, which is consistent with the observation of strong dissipation within the *a-b* planes. The optical properties for light polarized along the *c* axis reveal an insulating character dominated by lattice vibrations, superimposed on a weak electronic background. No Josephson plasma edge is observed in the low-frequency reflectance along the *c* axis for $x = 1/8$; however, sharp plasma edges are observed for $x = 0.095$ and 0.145 below T_c.

DOI: 10.1103/PhysRevB.85.134510 PACS number(s): 74.25.Gz, 74.72.Gh, 78.30.−j

I. INTRODUCTION

The discovery of superconductivity at elevated temperatures in the copper-oxide materials a quarter of a century ago sparked an intense effort to understand the mechanism of the superconductivity in these compounds. Despite the wealth of information from the accumulation of hundreds of thousands of scientific papers, there is still no consensus on the pairing mechanism. While superconductivity was originally observed in the single-layer $La_{2-x}Ba_xCuO_4$ system,[1] single crystals of this material proved difficult to grow and attention quickly shifted to the related $La_{2-x}Sr_xCuO_4$ materials where large single crystals were available. Further investigations into systems with more than two copper-oxygen layers in the unit cell led to rapid increases in the critical temperature (T_c), with the current maximum $T_c \simeq 135$ K observed at ambient pressure in the $HgBa_2Ca_2Cu_3O_{8+\delta}$ system.[2] The physical properties of this class of correlated electron materials and the nature of the superconductivity have been described in numerous review articles.[3–10] While most high-temperature superconductors display a doping-dependent dome-shaped superconducting phase boundary,[11–14] an anomalous weakening of the superconductivity is observed at a doping of $p = 1/8$ per copper atom in the related $La_{2-x}Sr_xCuO_4$ system,[15,16] and more recently in the $Bi_2Sr_2CaCu_2O_{8+\delta}$ and $YBa_2Cu_3O_{7-\delta}$ materials.[17,18] This so-called "1/8 anomaly" increases dramatically in $La_{2-x}Ba_xCuO_4$ for $x = 1/8$ and results in the almost total destruction of the bulk three-dimensional (3D) superconductivity.[15] There is also a structural transition over much of the phase diagram from a low-temperature orthorhombic (LTO) to a low-temperature tetragonal (LTT) symmetry[19–22] that is not observed in pure $La_{2-x}Sr_xCuO_4$ crystals; the LTO→LTT transition is also accompanied by the formation of an antiferromagnetically (AFM) ordered state.[23–25]

Recently, large single crystals of $La_{2-x}Ba_xCuO_4$ have become available that have allowed a much more detailed investigation of the electronic[26–35] and structural[36–47] properties of the 1/8 phase. With the onset of the LTT phase both long-range charge-stripe order, followed by spin-stripe order at a slightly lower temperature, are observed.[37] The question of what role stripes play in the formation of a superconducting state in the cuprate materials is the subject of some debate;[48–53] however, in this case, it appears that the formation of static charge-stripe order has the effect of electronically decoupling the copper-oxygen planes, significantly increasing the resistance along the *c* axis, and frustrating the formation of a bulk superconducting ground state.[54,55] The 1/8 phase exhibits a pseudogap[5] in the LTO phase,[56,57] similar to what is observed in the underdoped cuprates.[58] The remaining Fermi arc (or pocket) in the nodal region becomes gapped in the LTT phase close to the spin-ordering temperature. The gap in the nodal region is momentum-dependent with a *d*-wave form, $\Delta(\phi) = \Delta_0 \cos 2\phi$, where Δ_0 is the gap maximum and ϕ is a Fermi surface angle, similar to the form of the superconducting gap observed in other cuprate superconductors.[59,60] It has been proposed that this is a superconducting gap, but that the pairs lack the necessary phase coherence required to form a condensate.[28,29]

The optical properties of a material can provide important information about the nature of the lattice vibrations and the electronic transport, including the formation of charge and superconducting energy gaps. The role of charge-stripe and spin-stripe ordering in the 1/8 phase is of particular interest. Previous optical investigations of stripe correlations in an analogous phase of $La_{1.88-y}Nd_ySr_{0.12}CuO_4$[61–63] and in

$La_{2-x}Sr_xCuO_4$[63–65] have resulted in some disagreement over the association of certain infrared spectral features with charge order.[66,67]

In this work, we determine the temperature dependence of the optical properties of single crystals of $La_{2-x}Ba_xCuO_4$ over a wide frequency range for three different dopings, $x = 0.095$, 0.125, and 0.145 with T_c's of approximately 32, 2.4, and 24 K, respectively, for light polarized in the conducting a-b planes, and along the poorly conducting c axis. The optical conductivity in the a-b planes for all three materials show a Drude-like metallic behavior for the free carriers at room temperature with a scattering rate that decreases with temperature; for the superconducting $x = 0.095$ and 0.145 samples, there is a characteristic suppression of the low-frequency conductivity below T_c, allowing the superfluid density ρ_{s0} to be determined from this so-called missing spectral weight.[68] In contrast, in a refinement of earlier optical work,[26,69] the 1/8 phase shows a dramatic narrowing of the free-carrier response below T_{so} accompanied by the transfer of some spectral weight to both high and low frequencies. This transfer of spectral weight is consistent with the formation of a momentum-dependent gap due to the formation of charge-stripe and spin-stripe order resulting in a nodal metal. The loss of low-frequency spectral weight also mimics the missing spectral weight observed in the superconducting materials, and it is possible that the transfer of spectral weight is associated with the two-dimensional (2D) fluctuating superconducting state prior to the onset of bulk 3D superconductivity.[29] The two dopings for which superconductivity is observed fall on the universal scaling line, $\rho_{s0}/8 \simeq 4.4\,\sigma_{dc}\,T_c$ (where σ_{dc} is measured just above T_c),[70–73] which is consistent with the observation that there is substantial dissipation in the normal state of these materials.

The optical properties along the poorly-conducting c axis are dominated by the infrared-active lattice modes superimposed on a weak electronic background. In the superconducting $x = 0.095$ and 0.145 samples, sharp plasma edges in the low-frequency reflectance develop below T_c due to Josephson coupling between the planes. No Josephson plasma edge, or any indication of metallic behavior, is observed for the 1/8 phase down to the lowest measured temperature, despite the dramatic reduction of the c-axis resistivity below T_{so}.

II. EXPERIMENT

Single crystals of $La_{2-x}Ba_xCuO_4$ were grown using the traveling-solvent floating-zone method for a series of three nominal Ba concentrations, $x_0 = 0.095$, 0.125, and 0.155. The $x_0 = 0.095$ and 0.155 compositions are superconducting with transitions at $T_c \simeq 32$ and 24 K; the superconductivity in the $x = 0.125$ sample is strongly suppressed with $T_c \lesssim 2.4$ K (all values for T_c were determined by magnetic susceptibility). The T_c for the nominal $x_0 = 0.155$ crystal studied here (and in Ref. 69) is substantially lower than that of the piece (from the same growth) characterized in Ref. 46. Interpreting the discrepancy in T_c as a difference in Ba concentration, we estimate that the present sample corresponds to $x = 0.145 \pm 0.01$, and we refer to it as $x = 0.145$ throughout the rest of the paper.

The phase diagram of $La_{2-x}Ba_xCuO_4$ shown in Fig. 1(a) is considerably more sophisticated than that of the related

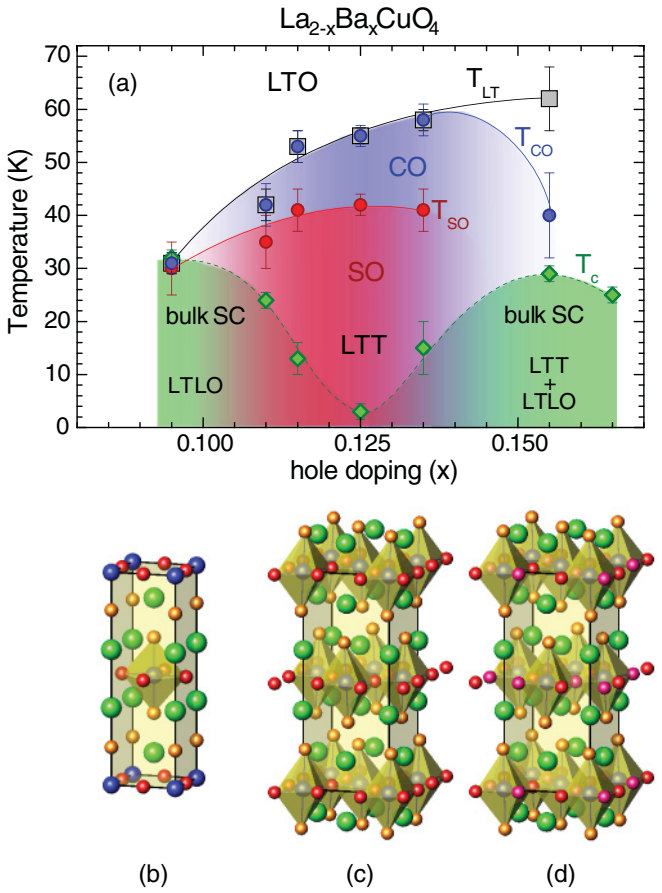

FIG. 1. (Color online) (a) Temperature vs hole doping phase diagram of $La_{2-x}Ba_xCuO_4$ single crystals (reproduced from Ref. 46). Onset temperatures: T_c for bulk superconductivity (SC), T_{co} for charge stripe order (CO), T_{so} for spin stripe order (SO), and T_{LT} for the low-temperature structural phases LTT and LTLO. The unit cell of $La_{2-x}Ba_xCuO_4$ is shown in the (b) high-temperature tetragonal (HTT), (c) low-temperature orthorhombic (LTO), and (d) low-temperature tetragonal (LTT) phases.

$La_{2-x}Sr_xCuO_4$ material.[46] Above room temperature, this material is in the $I4/mmm$ tetragonal (HTT) phase [see Fig. 1(b)]. With decreasing temperature, it undergoes an orthorhombic distortion into a $Bmab$ (LTO) phase [see Fig. 1(c)], which may be described as a tilting of the CuO_6 octahedra toward the La ions leading to a roughly $\sqrt{2} \times \sqrt{2}$ larger basal plane rotated by 45°. The HTT→LTO transition occurs at $T_{LTO} \simeq 305$, 235, and 190 K for the $x = 0.095$, 0.125, and 0.145 materials, respectively.[46] At dopings close to $x = 0.125$, the tilt of the octahedra moves between the La ions and is accompanied by a weak in-plane distortion resulting in a low-temperature tetragonal (LTT) phase $P4_2/ncm$ [see Fig. 1(d)]; this phase is associated with the development of charge-stripe and spin-stripe order.[74] In the $x = 0.095$, crystal close to $T_{co} \simeq T_{so} \simeq T_c$ the LTO structure undergoes a weakening of the orthorhombic strain, leading to a "low-temperature less orthorhombic" (LTLO) $Pccn$ phase at very low temperature.[34] In the $x = 0.145$ material, the LTO→LTT transition occurs at ≃62 K, but charge order does not develop until $T_{co} \simeq 56$ K and the spin order is likely very weak and is not observed;

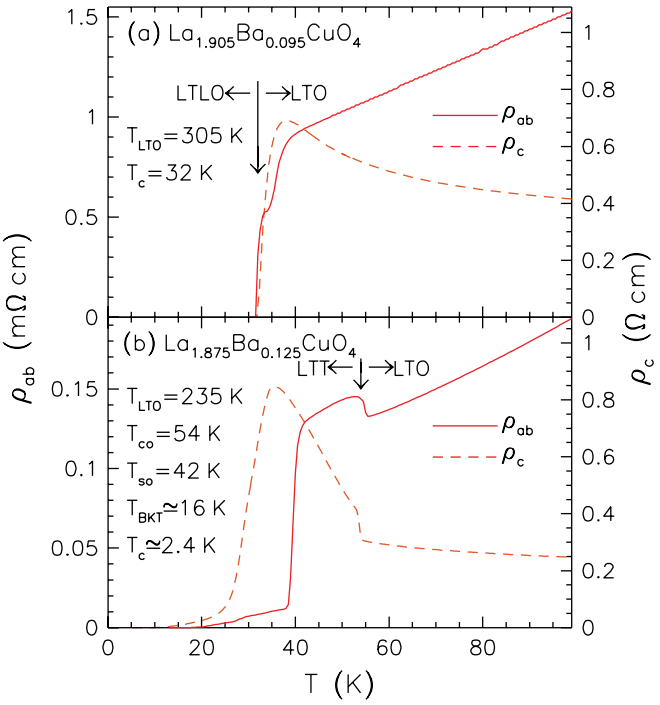

FIG. 2. (Color online) (a) The temperature dependence of the *ab*-plane (solid line) and *c*-axis (dashed line) resistivities for $x = 0.095$ (Ref. 34). In the normal state, ρ_{ab} decreases linearly with decreasing temperature, while ρ_c is observed to increase until just above T_c, below which both decrease dramatically and a weak anomaly is observed in ρ_{ab}. (b) The *ab*-plane and *c*-axis resistivities for the $x = 0.125$ material (see Refs. 28 and 29). Weak anomalies are observed in ρ_{ab} and ρ_c at T_{co}; ρ_{ab} continues to decrease until T_{so}, below which it falls dramatically before once again adopting a linear-temperature dependence. Along the *c* axis, ρ_c continues to increase below T_{co} until just below T_{so} where it begins to decrease quickly until $\simeq$25 K, below which it decreases less rapidly. Note different scales for ρ_{ab}.

at low temperature the structure is thought to be a mixture of LTT + LTLO.

The *ab*-plane and *c*-axis resistivities of the $x = 0.095$ material are shown close to $T_c \simeq 32$ K in Fig. 2(a) (Ref. 34). In the normal state ρ_{ab} displays a characteristic linear decrease with temperature, until just above T_c where a weak anomaly is observed that is associated with the onset of the structural transition previously described.[46,75] In contrast, in the normal state ρ_c increases with decreasing temperature, leading to a resistivity anisotropy ρ_c/ρ_{ab} that continues to increase until just above T_c. The *ab*-plane and *c*-axis resistivities of the $x = 0.125$ material are shown in Fig. 2(b) (see Refs. 28 and 29). In the normal state, ρ_{ab} decreases with temperature in an approximately linear fashion until a small jump is observed at the charge-ordering temperature ($T_{co} \simeq 54$ K), followed by a dramatic decrease at the spin-ordering temperature ($T_{so} \simeq 42$ K); this latter transition is extremely sensitive to the applied magnetic field.[28] Below T_{so}, a 2D fluctuating superconducting state is thought to form and the resistivity continues to decrease exponentially; at the same time, a strong diamagnetic response is observed.[29] This material is conjectured to undergo a Berezinskii-Kosterlitz-Thouless transition[76,77] at $T_{BKT} \simeq$ 16 K, below this temperature the resistivity is effectively zero.[28] A true bulk (3D) superconducting transition is finally achieved at $T_c \simeq 2.4$ K. In the normal state, ρ_c shows little change with decreasing temperature until T_{co} where, similar to ρ_{ab}, a small jump is observed; however, ρ_c continues to increase indicating a dramatic increase in the resistivity anisotropy until slightly below T_{so}, where ρ_c begins to decrease quickly, reaching a negligible value below $\simeq$6 K.[29]

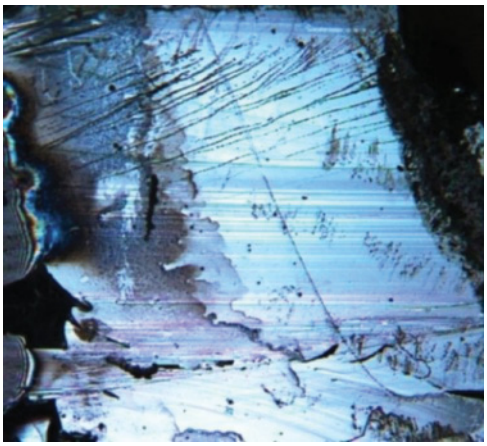

FIG. 3. (Color online) A photomicrograph of the cleaved *ab*-plane surface of $La_{1.875}Ba_{0.125}CuO_4$ revealing a number of striations and cleavage steps; the total area shown is roughly 2 mm × 2 mm.

It is possible to cleave some of these materials, resulting in mirror-like *ab*-plane surfaces. However, in most cases, cleaving yields a "terraced" surface consisting of numerous steps with exposed *c*-axis faces, shown in Fig. 3. In Fig. 4(a), the absolute reflectance of a freshly cleaved *ab*-plane surface for the $x = 0.095$ material has been measured at room temperature at a near-normal angle of incidence over the infrared region using an *in situ* evaporation technique.[78,79] In addition to the Hagen-Rubens $R \propto 1 - \sqrt{\omega}$ behavior expected for a metallic system and the two normally infrared-active vibrations at about 120 and 360 cm^{-1}, there are two strong antiresonances at $\simeq$460 and 575 cm^{-1} associated with the longitudinal optic modes of the infrared-active *c*-axis modes (see Sec. III B). These features are absent from naturally grown crystal faces, but are observed whenever a surface has been cut and polished, or as illustrated in the photomicrograph shown in Fig. 3, when a cleaved surface has numerous steps. This phenomenon has been documented extensively in the literature and is attributed to the misorientation of the *ab*-plane surface.[80–85]

Clearly, it is desirable to minimize these extrinsic features while preserving the intrinsic behavior of the sample. Pursuing this goal, the opposite face was polished using a series of successively finer diamond grits using kerosene as a suspension agent, with a final lap using a 0.1 μm diamond paste. The infrared reflectance shown in Fig. 4(b) is quite similar to the reflectance of the cleaved surface, and shows that the antiresonance features are still present. It was subsequently determined from x-ray Laue diffraction that this surface was misoriented by $\simeq 4^\circ$. The sample was reoriented using the Laue camera to better than 1° and then repolished. The resulting reflectance in Fig. 4(c) indicates that the antiresonance features have been minimized. Thus, while

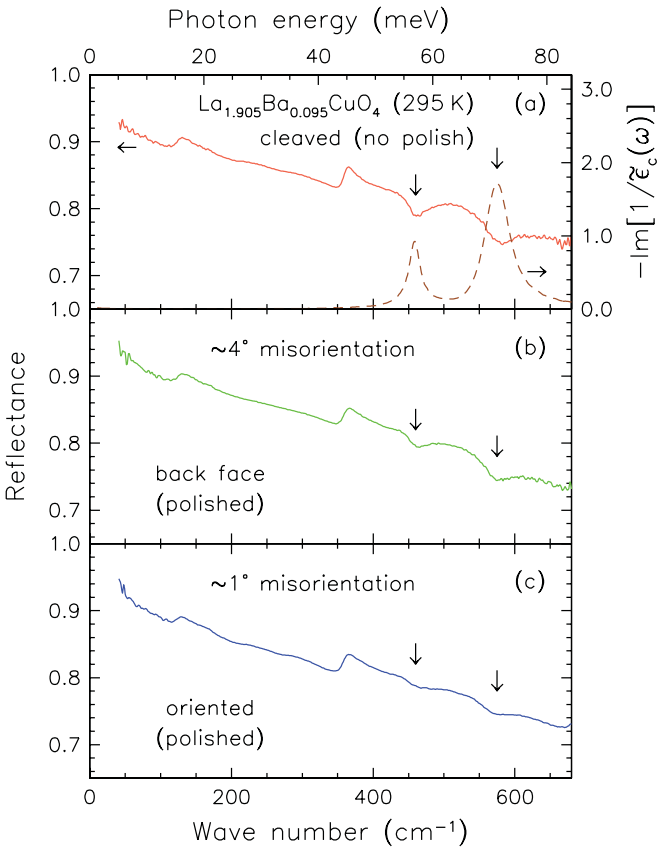

FIG. 4. (Color online) The reflectance of $La_{1.905}Ba_{0.095}CuO_4$ at 295 K in the far-infrared region for light polarized in the *a-b* planes. (a) The reflectance from a cleaved surface. There are two prominent antiresonances at $\simeq$460 and 570 cm^{-1}, which are associated with *c*-axis longitudinal optic modes that become infrared-active due to a surface misorientation. This effect can be seen in the *c*-axis loss function (dashed line). (b) The reflectance from the polished surface of the same sample with a measured surface misorientation of 4°; the antiresonances are still prominent. (c) The reflectance from the polished surface with a measured surface misorientation of $\lesssim$1°; the antiresonances are substantially weaker.

cleaved surfaces are often desirable, in those cases where strong antiresonances are observed, determining the correct orientation and careful polishing may remove most of these unwanted spectral features.

The reflectance of single crystal $La_{2-x}Ba_xCuO_4$ for $x =$ 0.095, 0.125, and 0.145 has been measured at a near-normal angle of incidence for light polarized in the *a-b* planes, as well as along the *c* axis, over a wide frequency range from $\simeq$2 meV to over 3 eV ($\simeq$20 to over 24 000 cm^{-1}) at a variety of temperatures using the previously described overcoating technique. The *ab*-plane reflectance of the $x =$ 0.125 sample was measured from a cleaved surface, while for the other dopings the surface was oriented to better than 1° and polished. The *c* axis was revealed by cutting the *a-b* face at 90°, which was subsequently polished. The *c* axis direction was determined by using an infrared polarizer to check the modulation of the infrared signal, with the minima corresponding to the *c*-axis direction.

The reflectance is a complex quantity consisting of an amplitude and a phase, $\tilde{r} = \sqrt{R}\exp(i\theta)$. Because only the amplitude $R = \tilde{r}\,\tilde{r}^*$ is measured in this experiment, it is often difficult to decipher how the reflectance is related to the real and imaginary optical properties. Thus the complex optical properties have been calculated from a Kramers-Kronig analysis of the reflectance.[86] The Kramers-Kronig transform requires that the reflectance be determined for all frequencies, thus extrapolations must be supplied in the $\omega \to 0,\infty$ limits. At low frequency, for light polarized in the *a-b* planes, above T_c in the normal state the metallic Hagen-Rubens form for the reflectance $R(\omega) \propto 1 - \sqrt{\omega}$ is employed. Below T_c in the superconducting state, $R(\omega) \propto 1 - \omega^4$; however, it should be noted that when the reflectance is close to unity the analysis is not sensitive upon the choice of low-frequency extrapolation. For light polarized along the *c* axis, at low frequency, the Hagen-Rubens form is used in the normal state, while below T_c we again use $R(\omega) \propto 1 - \omega^4$. For all polarizations, the reflectance is assumed to be constant above the highest measured frequency point up to $\simeq 1 \times 10^5$ cm^{-1}, above which a free electron gas asymptotic reflectance extrapolation $R(\omega) \propto 1/\omega^4$ is employed.[87]

III. RESULTS AND DISCUSSION

A. *a-b* plane

The temperature dependence of the reflectance of $La_{2-x}Ba_xCuO_4$ for light polarized in the *a-b* planes is shown over a wide frequency range for $x = 0.095, 0.125$, and 0.145 in Figs. 5(a)–5(c), respectively; the insets show the temperature dependence of the reflectance in the far-infrared region.

At room temperature, the reflectance curves for all three dopings are similar in that the reflectance at low frequency is high and decreases with frequency until a plasma edge in the reflectance is encountered at about 1 eV. The reflectance in the infrared region is observed to increase with electronic doping. In the three samples, the temperature dependence of the reflectance all show a similar increase in the low-frequency reflectance with decreasing temperature. In the superconducting state, the $x = 0.095$ material displays an abrupt increase in the low-frequency reflectance, while the changes in the $x = 0.145$ material below T_c are not as pronounced. At low temperature, the reflectance of the $x = 0.125$ sample is dramatically different; below $\simeq$200 cm^{-1} the reflectance increases down to the lowest measured temperature, but close to or below T_{so} the reflectance in the 200–2000 cm^{-1} region actually decreases with temperature,[26] as shown in the inset of Fig. 5(b). While the reflectance contains a great deal of information about the electronic transport and structure in a material, the complicated behavior observed in the $x = 0.125$ material makes it difficult to interpret. The determination of the optical conductivity from a Kramers-Kronig analysis of the reflectance is more revealing.

1. $x = 0.095$

The real part of the optical conductivity for light polarized in the *a-b* planes of $La_{1.905}Ba_{0.095}CuO_4$ is shown in the infrared region at temperatures above T_c in Fig. 6(a). At room temperature, the conductivity appears rather broad in the far-infrared region, but as the inset in this panel shows, it is in fact decreasing rather rapidly before giving way above

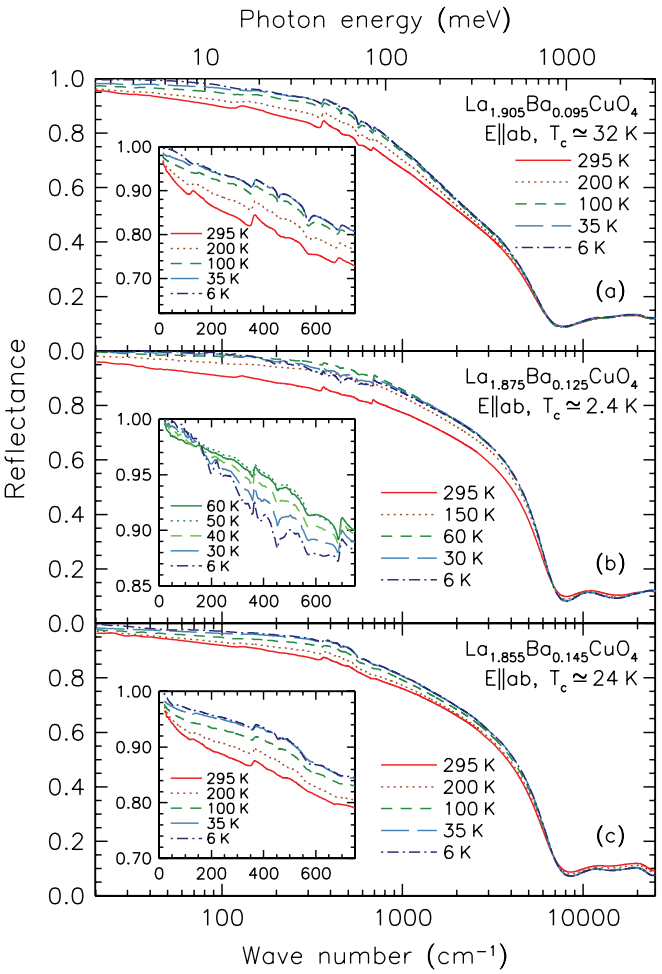

FIG. 5. (Color online) The temperature dependence of the reflectance of $La_{2-x}Ba_xCuO_4$ for light polarized in the a-b planes over a wide frequency range for (a) a polished sample with $x = 0.095$, (b) a cleaved sample for $x = 0.125$, and (c) a polished sample with $x = 0.145$. Insets: the temperature dependence of the reflectance in the far-infrared region.

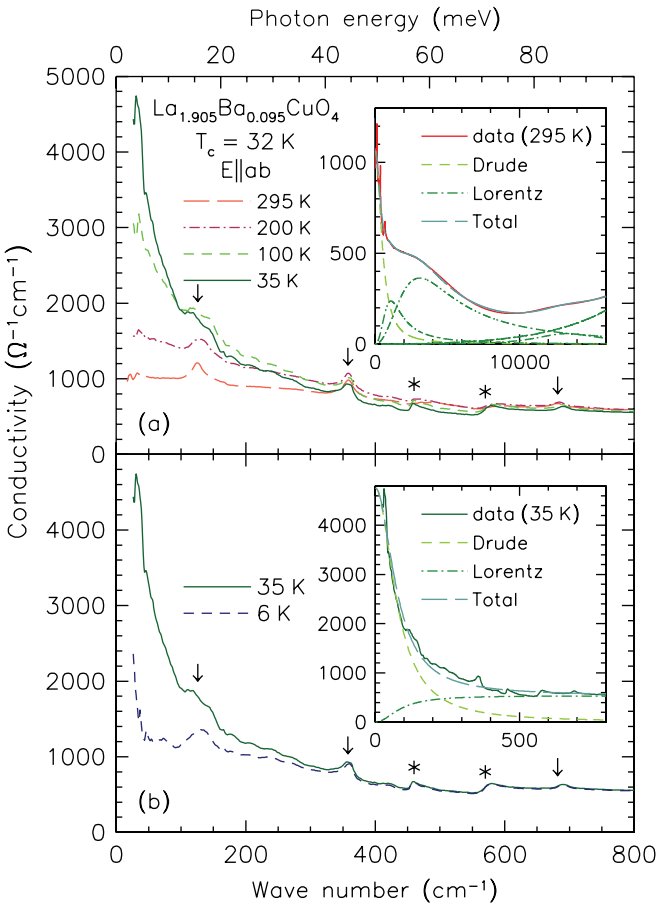

FIG. 6. (Color online) The real part of the optical conductivity of $La_{1.905}Ba_{0.095}CuO_4$ for light polarized in the a-b planes. (a) The infrared region for several temperatures above $T_c = 32$ K. The antiresonances observed in the reflectance in Fig. 4(c) are indicated by asterisks, while the in-plane infrared-active lattice modes are indicated by the arrows. Inset: the Drude-Lorentz fit to the data at 295 K. The Drude component (dashed line) and Lorentz oscillators (dash-dot lines) combine (long-dashed line) to reproduce the data (solid line) quite well. (b) The optical conductivity just above and well below T_c in the infrared region illustrating the transfer of spectral weight into the condensate. Inset: the Drude-Lorentz fit to the data at 35 K.

$\simeq$800 cm^{-1} to a broad plateau in the midinfrared; there is a shoulder at about 4000 cm^{-1} (0.5 eV) above which the conductivity continues to decrease until about 1 eV, at which point it begins to slowly rise again. Superimposed on the room-temperature conductivity curve are several sharp resonances at $\simeq$126, 358, and 682 cm^{-1}; these are the normally-active infrared vibrations that are observable due to the poor screening in this class of materials.[88] The weak antiresonances observed in the reflectance in Fig. 4(c) at $\simeq$460 and 570 cm^{-1} attributed to a surface misorientation manifest themselves as weak resonances or antiresonances in the conductivity. In the HTT phase, the irreducible vibrational representation for the infrared active modes is

$$\Gamma_{\rm IR}^{\rm HTT} = 4A_{2u} + 4E_u,$$

where the singly-degenerate A_{2u} modes are active along the c axis and the doubly-degenerate E_u modes are active in the a-b planes. Below the structural phase transition in the LTO phase, the unit cell is larger and more complicated. The lowered symmetry results in the removal of degeneracy and more infrared modes:

$$\Gamma_{\rm IR}^{\rm LTO} = 4A_u + 6B_{1u} + 7B_{2u} + 4B_{3u},$$

where the A_u modes are silent, and the singly-degenerate B_{1u}, B_{2u}, and B_{3u} modes are active along the c, b, and a axes, respectively. The additional low-temperature structural transition to either a LTLO or LTT + LTLO phase represents a further reduction of symmetry; for the LTT phase, the irreducible vibrational representation becomes

$$\Gamma_{\rm IR}^{\rm LTT} = 3A_{1u} + 7A_{2u} + 8B_{1u} + 3B_{2u} + 12E_u,$$

where the A_{1u}, B_{1u}, and B_{2u} modes are silent; as in the case of the HTT phase the A_{2u} and E_u modes are active along the c axis and the a-b planes, respectively.

At room temperature, $La_{1.905}Ba_{0.095}CuO_4$ appears to be in the HTT phase (demonstrated by the c-axis properties in Sec. III B); of four possible in-plane modes, only three are

clearly identified (the remaining mode is likely too weak to be observed). At low temperature, the vibrations typically narrow and increase in frequency; however, the low-frequency mode at $\simeq$126 cm^{-1} in Fig. 6(a) appears to broaden anomalously at low temperature, suggesting it may be sensitive to the charge or spin order.

As the temperature decreases, the low-frequency spectral weight associated with the free-carrier component increases rapidly. The spectral weight is defined here simply as the area under the conductivity curve over a given frequency interval: $N(\omega_c,T) = \int_{0^+}^{\omega_c} \sigma_1(\omega,T)\,d\omega$. For a metal, in the absence of other excitations, the area under the entire conductivity curve is the well-known f-sum rule,[89] $\int_0^\infty \sigma_1(\omega)\,d\omega = \omega_p^2/8$, where ω_p is the classical plasma frequency. The value for the dc resistivity for $x = 0.095$ in Fig. 2(a) just above T_c is in reasonably good agreement with the extrapolated value for $\sigma_{\rm dc} \equiv \sigma_1(\omega \to 0)$, although it should be noted that in this temperature region the resistivity is changing rapidly. Angle-resolved photoemission (ARPES) studies of high-temperature superconductors, in general, show a single band crossing the Fermi level,[7] indicating that the intraband excitations giving rise to the free-carrier component have a single origin. Within this context, it is not unreasonable to try and model the optical conductivity using a simple Drude-Lorentz model for the complex dielectric function $\tilde{\epsilon}(\omega) = \epsilon_1(\omega) + i\epsilon_2(\omega)$,

$$\tilde{\epsilon}(\omega) = \epsilon_\infty - \frac{\omega_{p,D}^2}{\omega^2 + i\omega/\tau_D} + \sum_j \frac{\Omega_j^2}{\omega_j^2 - \omega^2 - i\omega\gamma_j}, \quad (1)$$

where ϵ_∞ is the real part of the dielectric function at high frequency, $\omega_{p,D}^2 = 4\pi ne^2/m^*$ and $1/\tau_D$ are the square of the plasma frequency and scattering rate for the delocalized (Drude) carriers; ω_j, γ_j, and Ω_j are the position, width, and strength of the jth vibration or excitation. The complex conductivity is $\tilde{\sigma}(\omega) = \sigma_1(\omega) + i\sigma_2(\omega) = -i\omega[\tilde{\epsilon}(\omega) - \epsilon_\infty]/4\pi$, yielding the expression for the real part of the optical conductivity

$$\sigma_1(\omega) = \frac{1}{60}\,\frac{\omega_{p,D}^2\tau_D}{1+\omega^2\tau_D^2} + \sigma_{\rm MIR}, \quad (2)$$

where the first term is the Drude response and $\sigma_{\rm MIR}$ is the contribution from the bound (Lorentz) excitations. (When $\omega_{p,D}$ and $1/\tau_D$ are in units of cm^{-1}, the conductivity has units of Ω^{-1}cm^{-1}.) The Drude-Lorentz model has been fit to the normal state conductivity using a nonlinear least-squares method at 295 and 35 K. In addition to the Drude component, two Lorentz oscillators have been included somewhat arbitrarily at $\simeq$800 and 3100 cm^{-1} to reproduce the observed midinfrared response.[90] The fit to the data at 295 K is in good agreement with the experimental data and is shown over a broad spectral range in the inset of Fig. 6(a). The fit to the data in the normal state at 35 K is quite good and is shown in the inset in Fig. 6(b). The Drude plasma frequency $\omega_{p,D} \simeq 4360 \pm 300$ cm^{-1} does not vary with temperature, while the scattering rate decreases dramatically with temperature, $1/\tau_D \simeq 295$, 207, 131, and 75 cm^{-1} at 295, 200, 100, and 35 K, respectively (see Table I).

For a superconductor with an isotropic energy gap Δ, the gap in the optical conductivity is 2Δ. In the superconducting state below T_c, shown in Fig. 6(b) for $x = 0.095$, the dramatic decrease in the low-frequency optical conductivity below $\sim$200 cm^{-1} (25 meV) is associated with the formation of a superconducting energy gap;[68] this result is in reasonable agreement with the ARPES estimate of $2\Delta_0 \simeq 20$ meV for the maximum gap value in this material.[56,57] The "missing area" is referred to as the spectral weight of the condensate N_c and may be calculated from the Ferrell-Glover-Tinkham sum rule,[91,92]

$$N_c \equiv N(\omega_c, T \simeq T_c) - N(\omega_c, T \ll T_c) = \omega_{p,S}^2/8. \quad (3)$$

Here, $\omega_{p,S}^2 = 4\pi n_s e^2/m^*$ is the square of the superconducting plasma frequency, and the superfluid density is simply $\rho_{s0} \equiv \omega_{p,S}^2$; the cutoff frequency ω_c is chosen so that the integral converges smoothly. The superconducting plasma frequency has also been determined from the real part of the dielectric function in the low-frequency limit where $\epsilon_1(\omega) = \epsilon_\infty - \omega_{p,S}^2/\omega^2$. Yet another method of extracting $\omega_{p,S}$ from $\epsilon_1(\omega)$ is to determine $[-\omega^2\epsilon_1(\omega)]^{1/2}$ well below T_c in the $\omega \to 0$ limit.[93] All three techniques yield $\omega_{p,S} \simeq 3550 \pm 200$ cm^{-1}, which corresponds to an effective penetration depth of $\lambda_0 \simeq 4480 \pm 270$ Å. The fact that less than two-thirds of the free carriers in the normal state have condensed ($\omega_{p,S}^2/\omega_{p,D}^2 \lesssim 0.6$) is consistent with the observation of strong dissipation in the normal state.

TABLE I. The parameters for the Drude plasma frequency $\omega_{p,D}$ and scattering rate $1/\tau_D$ determined in the normal state at 100 K.[a] The superconducting plasma frequency $\omega_{p,S}$ and effective penetration depth are determined for $T \ll T_c$.

x	T_c (K)	$\omega_{p,D}$ (cm^{-1})	$1/\tau_D$ (cm^{-1})	$\omega_{p,S}$ (cm^{-1})	λ_0 (Å)
0.095	32	4360	131	3550	4480
0.125	$\sim$ 2.4	6480	105	–	–
0.145	24	7360	261	$\sim$2970	$\sim$5360

[a]Fits at 100 K; $x = 0.125$ interpolated from 60 and 150 K data.

2. $x = 0.145$

The temperature dependence of the real part of the optical conductivity for the $x = 0.145$ material is shown in Fig. 7 at a variety of temperatures above and below T_c. In the normal state, the overall behavior is not unlike that of the $x = 0.095$ material; at low frequency, a Drude-like component narrows rapidly with decreasing temperature but gives way to a broad, incoherent component above $\sim$60 meV. The conductivity in the normal state can be fit reasonably well using the Drude-Lorentz model yielding $\omega_{p,D} \simeq 7360$ cm^{-1} and $1/\tau_D \simeq 500$ cm^{-1} at room temperature. The larger value for $\omega_{p,D}$ denotes the increase in the density of free carriers. It is interesting to note that the normal-state scattering rate in the overdoped material is roughly twice that of the underdoped system; this may be due to electronic correlations or it may be that the increasing cation disorder in the blocking layer results in a larger value of $1/\tau_D$ (see Table I). Upon entry into the superconducting state a decrease in the low-frequency conductivity is once again observed; however, the onset at which this decrease occurs is rather indistinct and there is considerably more residual conductivity at low frequency than was observed in the underdoped material. Using the techniques previously discussed, the superconducting plasma frequency is estimated to be $\omega_{p,S} \simeq 2970 \pm 180$ cm^{-1}, corresponding to a penetration depth of $\lambda_0 \simeq 5360 \pm 350$ Å. As a result of the large normal

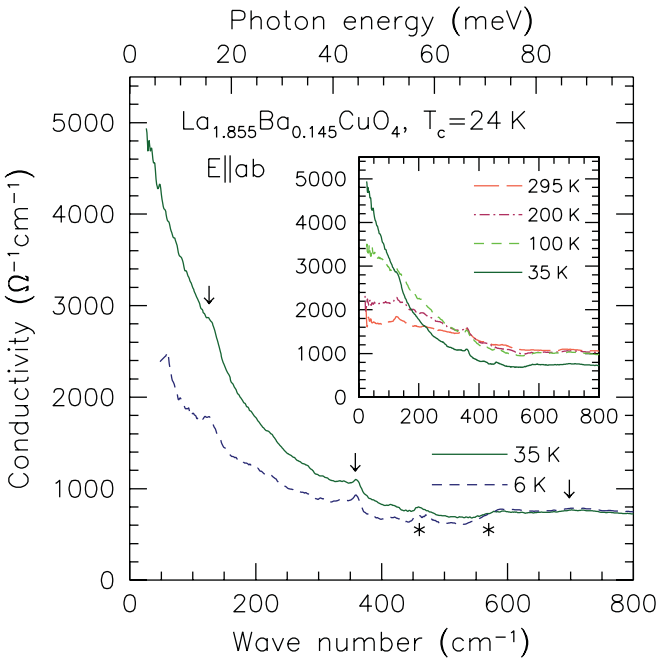

FIG. 7. (Color online) The real part of the optical conductivity of $La_{1.855}Ba_{0.145}CuO_4$ for light polarized in the a-b planes measured just above and well below the critical temperature. The asterisks denote structure due to surface misorientation, while the arrows indicate the in-plane infrared-active lattice modes. Inset: the temperature dependence of the optical conductivity in the normal state.

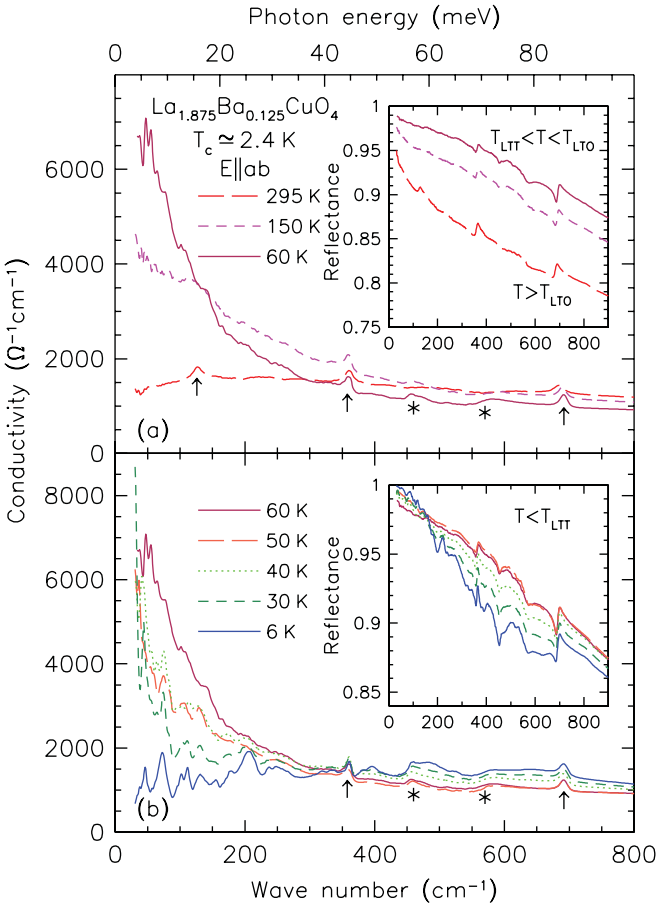

FIG. 8. (Color online) (a) The real part of the optical conductivity $La_{1.875}Ba_{0.125}CuO_4$ for light polarized in the a-b planes at several temperatures above T_{co} and T_{so}. Inset: the infrared reflectance for the same temperatures. (b) The conductivity for several temperatures below T_{co} and T_{so} in the same region showing the transfer and loss of spectral weight occurring mainly below T_{so}. Inset: the infrared reflectance for the same temperatures contrasting the different responses at low and high frequency. The asterisks denote structure due to surface misorientation, while the arrows indicate the in-plane infrared-active lattice modes.

state scattering rate, less than a fifth of the free-carriers have condensed ($\omega_{p,S}^2/\omega_{p,D}^2 \lesssim 0.2$).

3. $x = 0.125$

The in-plane reflectance of $La_{2-x}Ba_xCuO_4$ for $x = 0.125$ is shown in Fig. 5(b). While some aspects of the reflectance have been previously discussed,[26] there are several important points that bear repeating. As the temperature is lowered, the reflectance is observed to increase in the far- and midinfrared regions. Close to or below the spin-ordering temperature $T_{so} =$ 42 K, the reflectance decreases in the 200–2000 cm^{-1} interval; however, below about 200 cm^{-1} the reflectance continues to increase.[26] The consequences of this behavior may be seen more clearly in the conductivity shown for temperatures above T_{co} in Fig. 8(a) and mainly below T_{co} in Fig. 8(b). At high temperature, the optical conductivity can be modeled quite well using a Drude-Lorentz model; as the temperature is lowered from room temperature to just above $T_{co} = 54$ K, there is a characteristic narrowing of the Drude-like component and spectral weight is transferred from high to low frequency. The plasma frequency $\omega_{p,D} \simeq 6480 \pm 350$ cm^{-1} is relatively constant, while the scattering rate decreases from $1/\tau_D =$ 439 cm^{-1} at room temperature to 81 cm^{-1} at T_{co} (see Table I).

In Fig. 8(b), for $T_{so} < T < T_{co}$ the scattering rate continues to decrease without any obvious loss of spectral weight or change in $\omega_{p,D}$. Below T_{so}, the Drude-like component in the conductivity continues to narrow; however, above ~300 cm^{-1}, there is now a noticeable increase in the conductivity, indicating a transfer of spectral weight from the low-frequency free-carrier component to localized or gapped excitations,[94] the significance of which will be discussed in Sec. III C. This is precisely the temperature at which the infrared reflectance, shown in the inset of Fig. 8(b), begins to decrease above ≃200 cm^{-1}, while still increasing at low frequency. Below ≃30 K, little spectral weight is being transferred to high energy, instead the decrease in the low-frequency spectral weight is now associated almost entirely with the increasingly narrow free-carrier response, such as might be expected in a nodal metal.[95–97] Attempts to fit the free-carrier component with a Drude-model yield a rapidly decreasing value for $\omega_{p,D}$ for $T < T_{so}$, but at the same time $1/\tau_D$ is also decreasing dramatically.[26] We note that in the Drude model $\sigma_{dc} = \omega_{p,D}^2 \tau_D/60$, so that the net effect is the rapidly decreasing resistivity observed in Fig. 2(b). At ~6 K, the free-carrier response is now so narrow it may no longer be accurately observed, giving way to a broad, incoherent background conductivity. It is difficult to distinguish this behavior from the phenomenon of missing spectral weight in the superconducting state.

4. Scattering rate

The Drude model is a reasonable description of a noninteracting Fermi liquid; however, the cuprates are either moderately or strongly correlated electron systems.[98] In this latter case, a more general description of the Drude model is favored in which the scattering rate and the effective mass are allowed to adopt a frequency dependence:[99,100]

$$\frac{1}{\tau(\omega)} = \frac{\omega_p^2}{4\pi}\,\mathrm{Re}\left[\frac{1}{\tilde{\sigma}(\omega)}\right] \tag{4}$$

and

$$\frac{m^*(\omega)}{m_e} = \frac{\omega_p^2}{4\pi\omega}\,\mathrm{Im}\left[\frac{1}{\tilde{\sigma}(\omega)}\right], \tag{5}$$

where m_e is the bare mass, $m^*(\omega)/m_e = 1 + \lambda(\omega)$ and $\lambda(\omega)$ is a frequency-dependent electron-boson coupling constant. In this instance, we set $\omega_p \equiv \omega_{p,D}$ and $\epsilon_\infty = 4$ (although the choice of ϵ_∞ has little effect on the scattering rate or the effective mass in the far-infrared region). The infrared-active lattice modes observed in the conductivity have been fit using Lorentzian oscillators superimposed on a linear background and then removed from the complex dielectric function. The resulting temperature dependence of the in-plane scattering rate $1/\tau(\omega)$ is shown in Fig. 9 for the three different dopings studied in this work. A simple Drude model would produce a frequency-independent scattering rate; however, despite the reasonable agreement with the Drude model, in Figs. 9(a)–9(c), $1/\tau(\omega)$ displays an approximately linear frequency dependence. We note that in the $\omega \to 0$ limit the two models should yield the same scattering rate, and indeed $1/\tau(\omega \to 0) \simeq 1/\tau_D$.

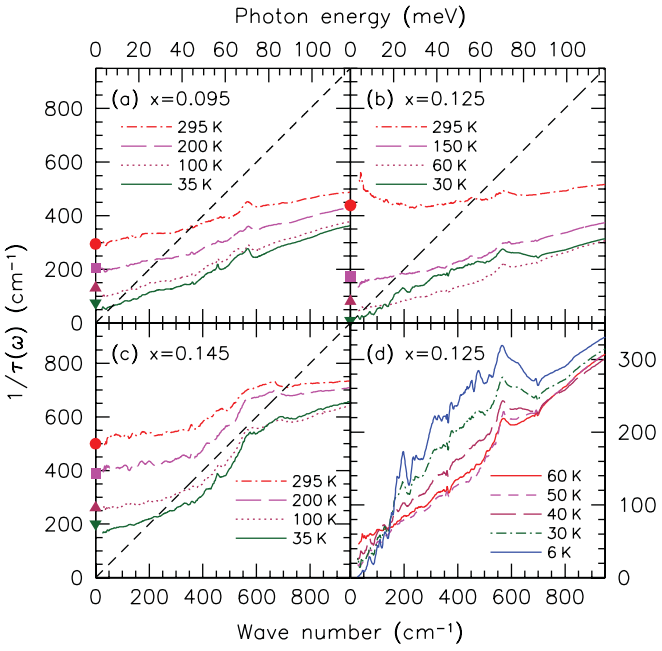

FIG. 9. (Color online) The temperature dependence of the in-plane frequency-dependent scattering rate in $La_{2-x}Ba_xCuO_4$ (with the phonons removed) in the far-infrared region for (a) $x = 0.095$, (b) the 1/8 phase, and (c) $x = 0.145$. (d) Detailed temperature dependence of the scattering rate for the 1/8 phase below 60 K. The values for $1/\tau_D$ determined from the Drude fits are indicated by the symbols at the origin. The dashed line indicates $1/\tau(\omega) = \omega$.

The temperature dependence $1/\tau_D$ (shown on the plots and for each doping) merits a brief discussion. For the three dopings examined, $x = 0.095$, 0.125, and 0.145, the values of the Drude scattering rate at 295 K increase steadily from $1/\tau_D = 295$ to 439 and 500 cm^{-1}, respectively, indicating either stronger electronic correlations or that the increase in barium concentration is accompanied by increasing out-of-plane cation disorder, which may in turn lead to an increase in elastic scattering in the copper-oxygen planes. While $1/\tau_D$ decreases reasonably quickly with decreasing temperature for $x = 0.095$, this trend is not as pronounced for $x = 0.145$. As previously noted, in the 1/8 crystal $1/\tau_D$ decreases steadily with temperature, but for $T < T_{so}$ the reduction of the scattering rate is dramatic, an effect that is shown in more detail in Fig. 9(d).

The frequency dependence of the scattering rate contains a wealth of information. The dashed line in Fig. 9 denotes $1/\tau(\omega) = \omega$; the region below this line is associated with a Landau-Fermi liquid regime where the quasiparticles are well defined. In the materials examined, at high temperature, $1/\tau(\omega) > \omega$ at low frequency, indicating that the conductivity in the *a*-*b* planes is strongly dissipative, and that the quasiparticles are not well defined. Across the far-infrared region $1/\tau(\omega)$ decreases with temperature and in the $x = 0.095$ material, just above T_c at 35 K, and in the 1/8 phase at low temperature ($T < T_{co}$), $1/\tau(\omega) \simeq \omega$, indicating well-defined quasiparticles and coherent transport; this condition is never satisfied in the $x = 0.145$ material. At low frequency, $1/\tau(\omega)$ decreases with decreasing temperature; however, in the 1/8 phase, this trend is reversed for $T \lesssim T_{so}$ above about 150 cm^{-1}, shown in Fig. 9(d), where the scattering rate increases dramatically. This behavior is consistent with the formation of a momentum-dependent gap.

It is interesting to note that, aside from some artifacts due to the imperfect nature of the phonon subtraction, for the $x = 0.095$ material in Fig. 9(a) the frequency-dependent scattering rate is essentially featureless except for a small kink at about 45 meV (also observed in the $x = 0.145$ material). In many high-temperature superconductors, $1/\tau(\omega)$ often has sharp inflection points in the normal state;[101] when an inversion of the scattering rate is performed[102,103] these structures correspond to peaks in the electron-boson spectral function.[104–106] It has been proposed that the peak location is proportional to the position of the magnetic scattering resonance[107,108] in polarized neutron scattering measurements $\Omega_r \approx 5.4\,k_B T_c$, and more generally that it scales with the superconducting transition temperature,[109] $\Omega_r \approx 6.3\,k_B T_c$. In the underdoped cuprates, the presence of a pseudogap on the Fermi surface is expected to produce kinks in the scattering rate at roughly $\Omega_r + \Delta_{pg}$ and $\Omega_r + 2\Delta_{pg}$.[110] In the $x = 0.095$ ($T_c = 32$ K) material, taking the average, $\Omega_r \simeq 16$ meV, while $\Delta_{pg} \simeq 15$ meV (see Ref. 56) yielding $\simeq$31 and 46 meV; the larger value is very close to where a kink is observed in $1/\tau(\omega)$ in Fig. 9(a). While it is tempting to associate this kink with a magnetic resonance, the absence of such a feature in the underdoped $La_{2-x}Sr_xCuO_4$ material[111,112] suggests a different origin for this feature. In the more heavily doped $x = 0.145$

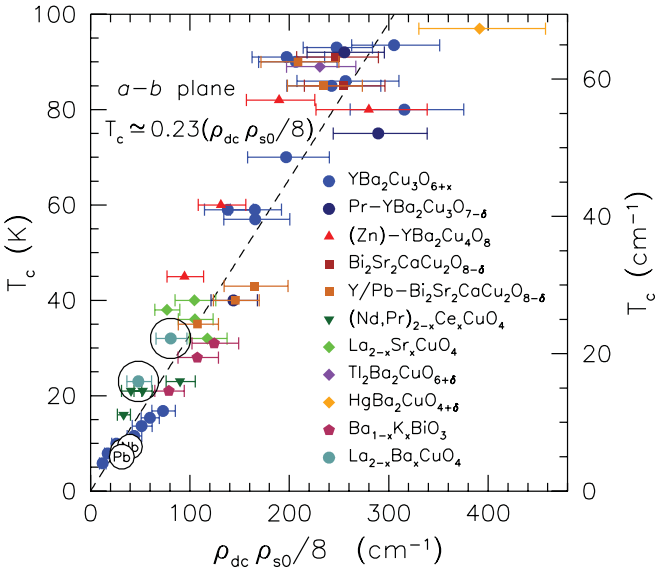

FIG. 10. (Color online) The critical temperature T_c vs the product of the dc resistivity measured just above T_c and the spectral weight of the condensate, $\rho_{dc}\,\rho_{s0}/8$, in the copper-oxygen planes for a variety of electron and hole-doped cuprates, compared with the a-b plane results for $La_{2-x}Ba_xCuO_4$ for $x = 0.095$ and 0.145 (highlighted within the circles). The dashed line corresponds to the general result for the cuprates $T_c \simeq 0.23\,(\rho_{dc}\,\rho_{s0}/8)$.

($T_c \simeq 24$ K) material, $\Omega_r \simeq 12$ meV and $\Delta_{pg} \simeq 10$ meV suggesting features at ≃22 and 32 meV; however, no obvious structure in the scattering rate is observed in Fig. 9(c) at either of these energies.

5. *Parameter scaling*

It has been noted that the high-temperature superconductors obey the scaling relation $\rho_{s0}/8 \simeq 4.4\,\sigma_{dc}\,T_c$, where $\sigma_{dc} = \sigma_1(\omega \to 0)$ is the dc conductivity in the normal state measured at $T \gtrsim T_c$, and the superfluid density ρ_{s0} is determined for $T \ll T_c$; this scaling relation is valid for both the metallic a-b planes as well as along the poorly conducting c axis, in both the electron- and hole-doped cuprates.[70–73] In this representation, the scaling relation is valid over five orders of magnitude and as such is usually shown as a log-log plot. However, when only the a-b plane results are considered, the results span less than two orders of magnitude and it is convenient to rewrite this relation as

$$T_c \simeq 0.23\,(\rho_{dc}\,\rho_{s0}/8), \tag{6}$$

where $\rho_{dc} = 1/\sigma_{dc}$. The scaling relation now has a similar appearance to the well-known Uemura relation,[113] $T_c \propto \rho_{s0}$, and may be shown using a linear scale. In Fig. 10, the values for T_c are plotted against $\rho_{dc}\,\rho_{s0}/8$ determined in the a-b planes for a variety of single-layer and double-layer cuprates. The values for $La_{2-x}Ba_xCuO_4$ for $x = 0.095$ ($T_c = 32$ K, $\sigma_{dc} = 4100 \pm 400\ \Omega^{-1}\text{cm}^{-1}$ just above T_c, and $\rho_{s0} = 12.6 \pm 1 \times 10^6$ cm^{-2}) and $x = 0.145$ ($T_c = 24$ K, $\sigma_{dc} = 4800 \pm 400\ \Omega^{-1}\text{cm}^{-1}$ just above T_c, and $\rho_{s0} = 8.8 \pm 0.8 \times 10^6$ cm^{-2}) are highlighted within the circles and fall on the general scaling line. These points also lie quite close to the related $La_{2-x}Sr_xCuO_4$ materials with comparable doping. This result is consistent with the observation that there is strong dissipation in the normal state.[114–117]

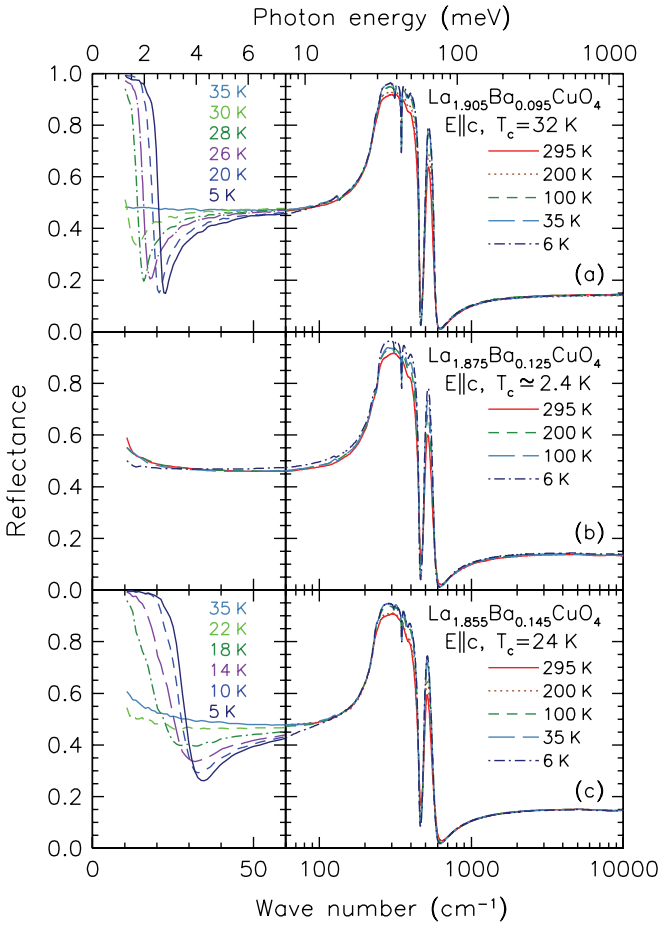

FIG. 11. (Color online) The temperature dependence of the reflectance of $La_{2-x}Ba_xCuO_4$ for light polarized along the c axis for (a) $x = 0.095$, (b) $x = 0.125$, and (c) $x = 0.145$. The wave number (photon energy) scale is linear up to 60 cm^{-1}; above this, it is logarithmic.

B. *c* axis

1. *Optical properties*

The temperature dependence of the reflectance of $La_{2-x}Ba_xCuO_4$ for light polarized along the poorly conducting c axis is shown in Figs. 11(a)–11(c) for the $x = 0.095$, 0.125, and 0.145 dopings, respectively. The reflectance in this polarization is dramatically different than what is observed in the metallic a-b planes (see Fig. 5); as a result of the near total absence of a free-carrier contribution to the dielectric function, the reflectance is dominated by the normally infrared-active c-axis lattice modes. In the normal state as $\omega \to 0$, the reflectance displays a slight upturn, indicative of a weakly conducting state; this is seen most clearly in the $x = 0.145$ material. Below T_c, a sharp plasma edge is observed in the reflectance at low frequency in Figs. 11(a) and 11(c) for the $x = 0.095$ and 0.145 dopings, respectively. The onset of the plasma edge is extremely rapid in both materials. The 1/8 phase material shows no hint of a plasma edge in the reflectance; however, this is not surprising as the bulk T_c in this

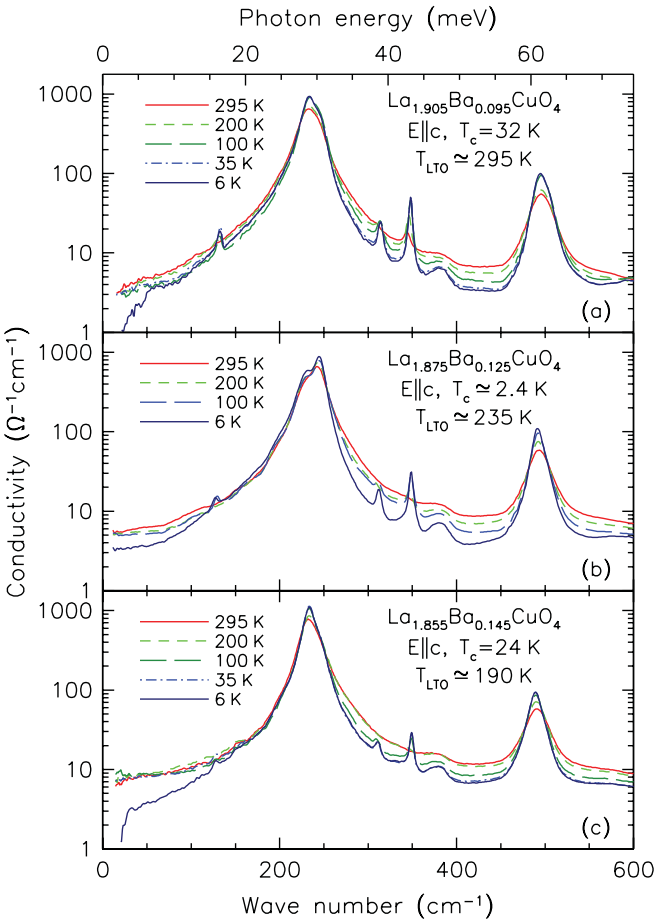

FIG. 12. (Color online) The temperature dependence of the real part of the optical conductivity of $La_{2-x}Ba_xCuO_4$ for light polarized along the poorly conducting c axis for (a) $x = 0.095$, (b) $x = 0.125$, and (c) $x = 0.145$.

material is too low to be accessed in our current experimental configuration.

The c-axis plasma edge in the reflectance is observed in many of the cuprate superconductors,[118–126] and is attributed to the Josephson coupling of the copper-oxygen planes resulting in the formation of a supercurrent and the onset of a bulk 3D superconducting state.[127–129] It is interesting to note that the Josephson plasma edge is considerably broader in the more heavily doped material; this observation is in agreement with the result for heavily doped $La_{2-x}Sr_xCuO_4$ where it is suggested that the smearing of the plasma edge is due to spatial variations of the superconducting condensate.[125]

The behavior along the c axis is easier to understand when the conductivity is considered, shown in Figs. 12(a)–12(c) for $x = 0.095$, 0.125, and 0.145, respectively. In each case, the conductivity is dominated by a very strong infrared lattice mode at $\simeq$235 cm^{-1} with another prominent mode at $\simeq$496 cm^{-1}; the conductivity is shown on a logarithmic scale to allow the emergence of weaker modes as well as the behavior of the electronic background to be examined. The results of oscillator fits to the conductivity for the $x = 0.095$ material at 295 and 35 K are listed in Table II.

In the HTT phase, a total of four A_{2u} modes are expected along the c axis; despite $T_{LTO} \simeq 305$ K in the $x = 0.095$ material, it is clear from the conductivity in Fig. 12(a) that only four modes at $\simeq$235, 344, 381, and 496 cm^{-1} are present at room temperature, indicating that the material is indeed in the HTT phase. For $T < T_{LTO}$, two new modes at $\simeq$133 and 314 cm^{-1} quickly emerge, in agreement with the six B_{1u} modes expected in the LTO phase. It is unclear what effect, if any, the LTLO phase would have on the nature of the c axis vibrations; however, at the lowest measured temperature, there is a slight asymmetry in the strong 235 cm^{-1} mode, suggesting a possible further reduction of symmetry. The vibrational properties in the $x = 0.125$ and 0.145 materials are similar. At room temperature, both of these materials are in the HTT phase and four modes are observed; two new modes emerge below the respective values for T_{LTO}. In the 1/8 phase, at $\sim$6 K, this material is expected to be in an LTT phase and a total of seven A_{2u} modes are expected to be active along the c axis; the shoulder in the strong 235 cm^{-1} mode suggests that all seven A_{2u} modes may be observed. The picture in the more heavily doped $x = 0.145$ material is less clear. While six modes are observed at low temperature as expected for the LTT phase, the modes in this material have broadened and it is no longer obvious if there is any asymmetry in the 235 cm^{-1} mode at low temperature. This may be a reflection of the somewhat ambiguous nature of the low-temperature structure (LTT+LTLO) for this doping.[46]

TABLE II. The vibrational parameters for oscillator fits to the infrared-active phonon modes observed along the c axis in $La_{1.905}Ba_{0.095}CuO_4$ at 295 K (HTT) and at 35 K (LTO), where ω_j, γ_j and Ω_j are the frequency, width and oscillator strength, respectively. The estimated errors are indicated in parenthesis. All units are in cm^{-1}.

Mode	ω_j	γ_j	Ω_j
	$T = 295$ K (HTT)		
A_{2u}	234.6 (0.2)	29 (0.6)	1085 (10)
A_{2u}	343.6 (0.1)	9.2 (0.5)	61 (4)
A_{2u}	381.0 (0.6)	34 (3)	71 (10)
A_{2u}	495.9 (0.1)	25 (0.6)	312 (5)
	$T = 35$ K (LTO)		
B_{1u}	132.7 (0.2)	5.7 (0.9)	55 (6)
B_{1u}	235.4 (0.2)	22 (0.6)	1110 (10)
B_{1u}	314.2 (0.1)	7.1 (0.2)	85 (2)
B_{1u}	348.0 (0.1)	4.6 (0.3)	113 (6)
B_{1u}	380.4 (0.9)	39 (6)	109 (13)
B_{1u}	495.8 (0.2)	19 (0.6)	338 (5)

The conductivity along the c axis is orders of magnitude lower than what is observed in the metallic a-b planes. At room temperature, in the $x = 0.095$ material $\sigma_{dc} \equiv \sigma_1(\omega \rightarrow 0) \simeq 3\ \Omega^{-1}$cm^{-1}, increasing to $\simeq$6 Ω^{-1}cm^{-1} in the 1/8 phase [both values are comparable with the c axis resistivity shown in Figs. 2(a) and 2(b)], and $\simeq$8 Ω^{-1}cm^{-1} in the $x = 0.145$ material. The normal-state transport along the c axis is attributed to thermally activated hopping, which is consistent with the observation of an electronic background that decreases (weakly) with temperature. In addition, some of this decrease in the optical conductivity may also be due to a narrowing of vibrational features.

Despite the small value for the background conductivity, a suppression of the low-frequency conductivity due to the

formation of a condensate is observed below T_c in the $x = 0.095$ and 0.145 materials. The decrease in the low-frequency conductivity in the 1/8 phase below T_{co} is likely due to the decoupling of the planes due to the formation of charge-stripe order;[34,54] however, the dramatic decrease in the c-axis resistivity below T_{so} [see Fig. 2(b)] is not reflected in the optical properties as no commensurate increase in the conductivity is observed down to the lowest measured frequency. This suggests that the decrease in the low-frequency spectral weight at low temperature is associated with an increase in the optical conductivity at very low energies (possibly microwave or radio frequencies), and is likely associated with the onset below T_{so} of superconducting correlations in the planes.[29] In the $x = 0.095$ and 0.145 compounds the energy scale for the loss of spectral weight is roughly 80 cm^{-1} (10 meV) and 140 cm^{-1} (18 meV), respectively. It is interesting to note that these energy scales correspond to Δ_0, rather than $2\Delta_0$ observed in the a-b planes.[56] This type of behavior has been previously observed in the cuprates;[130] however, it remains unexplained.

2. Penetration depth

While it is possible to determine $\omega_{p,S}$ from the Ferrell-Glover-Tinkham sum rule, the small values of the conductivity and the proximity of strong lattice vibrations can lead to significant uncertainties. Under these circumstances a more reliable approach is to examine the low-frequency response of the real part of the dielectric function, $\epsilon_1(\omega) = \epsilon_\infty - \omega_{p,S}^2/\omega^2$. For $T \ll T_c$, this method yields $\omega_{p,S} = 119 \pm 10$ cm^{-1} for $x = 0.095$ and $\omega_{p,S} = 174 \pm 14$ cm^{-1} for $x = 0.145$, which corresponds to effective penetration depths of approximately 13.4 and 9.1 μm, respectively. It is also possible to track the temperature dependence of the superfluid density using this method. The temperature dependence of the superfluid density for the $x = 0.095$ and 0.145 samples, expressed here as the ratio value of the square of the penetration depths $\lambda^2(0)/\lambda^2(T)$, is plotted against the reduced temperature $t = T/T_c$ and compared with optimally doped $La_{1.85}Sr_{0.15}CuO_4$, shown in Fig. 13. In a comprehensive study of the evolution of the c-axis superfluid density in $La_{2-x}Sr_xCuO_4$ for a wide variety of dopings,[126] it may be noted that the superfluid density develops most rapidly for the optimally doped material. It is therefore surprising that in underdoped $La_{1.905}Ba_{0.095}CuO_4$, the superfluid density develops extremely quickly just below T_c before slowing below $T_c/2$; in this regard, it is reminiscent of the behavior of a system with an isotropic s-wave energy gap,[131] while the more heavily doped $x = 0.145$ sample develops relatively slowly and is similar to what is observed in the copper-oxygen planes in a d-wave system.[132]

We attribute this difference in behavior to the presence of a pseudogap in the underdoped materials where the antinodal region is gapped well above T_c. If the c-axis transport is dominated by the antinodal zone boundary region of the Fermi surface,[133–135] then when the Fermi pocket is gapped below T_c, the c-axis response will be dominated by the gap maximum Δ_0 well away from the nodal region, and thus will not be sensitive to the d-wave nature of the system, instead resembling a more isotropic system.[72] The formation of charge order in the $x = 0.095$ material below ≃25 K may frustrate the Josephson coupling between the planes,[34] leading to the observed slowing

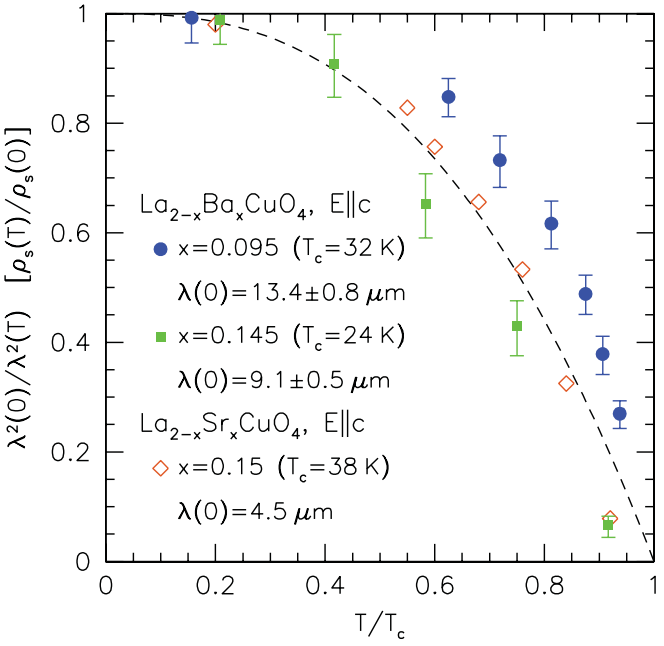

FIG. 13. (Color online) The temperature dependence of the superfluid density along the c axis normalized to an extrapolated zero-temperature value vs the reduced temperature, $t = T/T_c$, in $La_{2-x}Ba_xCuO_4$ for $x = 0.095$ (●) and 0.145 (■) and optimally-doped $La_{1.85}Sr_{0.15}CuO_4$ (◇) (see Ref. 126). The dashed line is a guide to the eye.

of the formation of the condensate below roughly $T_c/2$. On the other hand, the pseudogap is generally not present in materials close to optimal doping; below T_c, the entire Fermi surface is gapped. This suggests that in an optimally doped material the c-axis response will be more sensitive to the d-wave nature of the energy gap and therefore evolves more slowly, similar to the response observed in the copper-oxygen planes.[136]

3. Parameter scaling

It was previously noted that the scaling relation $\rho_{s0}/8 \simeq 4.4\,\sigma_{dc}T_c$ is valid not only in the a-b planes, but also along the c axis.[70] While it is possible to plot the c axis data in the form of T_c versus $\rho_{dc}\,\rho_{s0}/8$, the highly anisotropic nature of these materials results in conductivities (resistivities) along the c axis that are orders of magnitude smaller (larger) than those observed in the a-b planes, resulting in a significant uncertainty in $\sigma_{dc} = \sigma_1(\omega \to 0)$ and the corresponding value for $\rho_{dc} = 1/\sigma_{dc}$. In addition, the scaling behavior of ρ_{s0} emerges naturally if the superconductivity along the c axis is considered to originate from Josephson coupling.[72]

The c axis values for the spectral weight of the condensate $\rho_{s0}/8$ are plotted as a function of $\sigma_{dc}\,T_c$ in Fig. 14 for a variety of single-layer and double-layer cuprates. The dashed line is the best fit to the data, $\rho_{s0}/8 \simeq 4.4\,\sigma_{dc}\,T_c$. The c-axis values for $La_{2-x}Ba_xCuO_4$ for $x = 0.095$ ($T_c = 32$ K, $\sigma_{dc} = 3 \pm 1$ $\Omega^{-1}cm^{-1}$ just above T_c, and $\rho_{s0} = 1.4 \pm 0.2 \times 10^4$ cm^{-2}) and 0.145 ($T_c = 24$ K, $\sigma_{dc} = 9 \pm 2\,\Omega^{-1}cm^{-1}$ just above T_c, and $\rho_{s0} = 3.0 \pm 0.3 \times 10^4$ cm^{-2}) are highlighted in the circles. These values fall on the general scaling line and once again are quite close to the related $La_{2-x}Sr_xCuO_4$ materials with comparable doping.

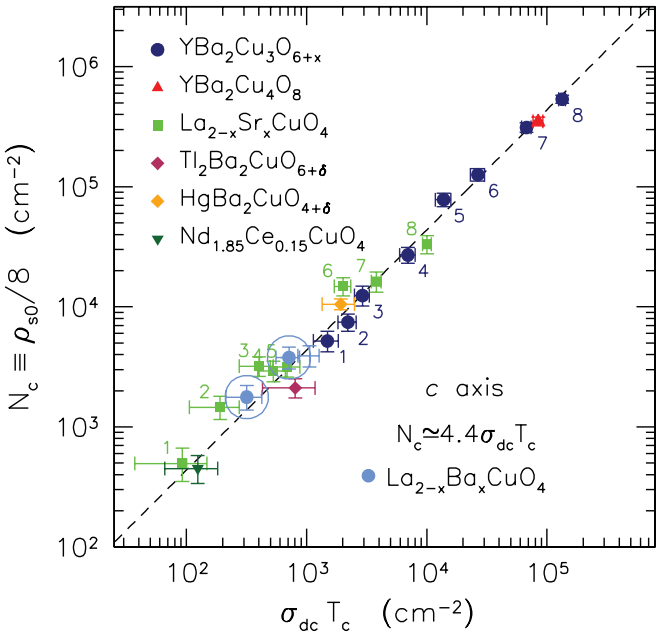

FIG. 14. (Color online) The log-log plot of the spectral weight of the superfluid density $N_c \equiv \rho_{s0}/8$ vs $\sigma_{\rm dc}\,T_c$ along the c axis for a variety of electron and hole-doped cuprates compared with $La_{2-x}Ba_xCuO_4$ for $x = 0.095$ and 0.145 (highlighted within the circles). The superscripts next to the symbols for $La_{2-x}Sr_xCuO_4$ and $YBa_2Cu_3O_{6+y}$ refer to different chemical dopings.[71] The dashed line corresponds to the general result for the cuprates $\rho_{s0}/8 \simeq 4.4\sigma_{\rm dc}T_c$.

C. The anomalous 1/8 phase

The behavior of the optical conductivity at low temperature in the $x = 1/8$ phase is fundamentally different than the other two dopings, where a response that is consistent with the opening of a superconducting d-wave energy gap is observed. The transfer of spectral weight from low to high frequency that develops close to or below $T_{\rm so}$ is extremely unusual for a hole-doped cuprate and has the characteristics of an anisotropic transport gap on the Fermi surface due to the formation of charge or spin order. A partial gapping of the Fermi surface has been observed in other 2D materials with incommensurate charge-density waves (CDW's).[137–140] Unlike one-dimensional systems, where the modulation wave vector can perfectly span the Fermi surface and the CDW almost always leads to the complete gapping of the Fermi surface, in 2D perfect nesting is not possible[141] and as a result, the CDW gaps only a portion of the Fermi surface. Fortunately, ARPES measurements have been performed on this composition,[56,57] so that we can analyze nesting of the Fermi surface by the measured modulation wave vectors.[46] The charge-order wave vector is approximately equal to $4k_{\rm F}$ in the antinodal region. There is certainly a gap on that portion of the Fermi surface, but it is already there as a pseudogap before the charge-stripe order appears.[56,57] Therefore the temperature dependence of the optical spectral weight transfer suggests a connection with the spin-stripe order for which the wave vector would nest parts of the Fermi arc. The ARPES measurements indicate that the gapping of the Fermi arc below $T_{\rm so}$ is indistinguishable from the d-wave-like gap found in superconducting samples.[56,57]

While the conventional density-wave picture is a possible candidate to explain the observed redistribution of spectral weight at low temperature, another possibility is that this shift is associated with superconducting correlations in this material.[29] We are not able to access the bulk superconducting state in the $x = 1/8$ material; however, the previously discussed scaling relation[70] indicates that because of the dramatically reduced value for the bulk superconductivity in this material ($T_c \simeq 2.4$ K) the Josephson plasma frequency along the c axis is estimated to be $\omega_{p,S} \simeq 17$ cm^{-1}. The Josephson plasma edge in the reflectance typically occurs in a region close to the renormalized superconducting plasma frequency $\tilde{\omega}_{p,S} = \omega_{p,S}/\sqrt{\epsilon_{\rm FIR}}$. Given the experimentally determined value of $\epsilon_{1,c} \simeq 30$ at 50 cm^{-1}, this yields a value of $\tilde{\omega}_{p,S} \simeq 3$ cm^{-1}, below our ability to measure using current optical techniques. The strongly reduced value for the c-axis Jopsephson plasma edge for $x = 1/8$ is consistent with the disappearance of this feature in $La_{1.85-y}Nd_ySr_{0.15}CuO_4$, which occurs when the increasing Nd concentration causes the structure to change from LTO to LTT, resulting in stripe order.[62,69] To explain the abrupt change in the Josephson coupling in the latter case, despite the much weaker reduction in T_c, Himeda *et al.*[142] proposed a pair-density-wave (PDW) superconducting state involving local d-wave symmetry but modulated by a sinusoidal envelope function; the envelope function has the same period as the spin modulation, but its extrema are aligned with the maxima of the charge modulation. The rotation of the stripe (and PDW) orientation by 90° from layer to layer leads to a frustration of the interlayer Josephson coupling. This concept was rediscovered[54,143] after the observation of quasi-two-dimensional superconductivity by transport measurements[28] on $La_{2-x}Ba_xCuO_4$ with $x = 1/8$.

The PDW proposal also has implications for the in-plane conductivity. Given a sinusoidally-modulated pair wave function, the superfluid density can be written as

$$\rho_s(\mathbf{r}) = 0.5\rho_s[1 + \cos(2\mathbf{q}\cdot\mathbf{r} + \phi)], \tag{7}$$

where $\mathbf{q} = (\frac{1}{8},0,0)$ [or $(0,\frac{1}{8},0)$] is the ordering wave vector (in reciprocal lattice units based on the HTT phase), and ϕ is the phase of the modulation with respect to the crystal lattice. Barabash *et al.*[144] showed that inhomogeneity of the superfluid density will cause some of the conductivity that would normally be at $\omega = 0$ to shift to finite ω. Orenstein[145] went further and showed that sinusoidal modulation of $\rho_s(\mathbf{r})$ shifts conductivity to a peak at the renormalized superconducting plasma frequency $\tilde{\omega}_{p,S} \approx \omega_{p,S}/\sqrt{\epsilon_\infty}$. From Table I, we extrapolate an in-plane value of $\omega_{p,S} \simeq 3250$ cm^{-1} for $x = 1/8$. Using the experimentally-determined value of $\epsilon_{1,a} \simeq 4$ at 2 eV for ϵ_∞ [there is little or no temperature dependence of $\epsilon_{1,a}(\omega)$ in this frequency region], then we estimate the in-plane $\tilde{\omega}_{p,S} \simeq 1600$ cm^{-1}. In considering Fig. 8(b), we already noted that some spectral weight is shifted from low frequency to above 300 cm^{-1}. To emphasize this behavior, Fig. 15 shows the ratio of $\sigma_1(\omega,T)$ to that at $T = 60$ K. The enhancement of σ_1 at ~80 meV is clearly present at 40 K and has doubled by 6 K; however, there is no enhancement at 50 K, which is already below $T_{\rm co}$. The development of the 80-meV feature on cooling correlates with the drop in in-plane resistivity.

To compare with Orenstein's analysis,[145] we have to allow for the fact that we have superconducting correlations but not

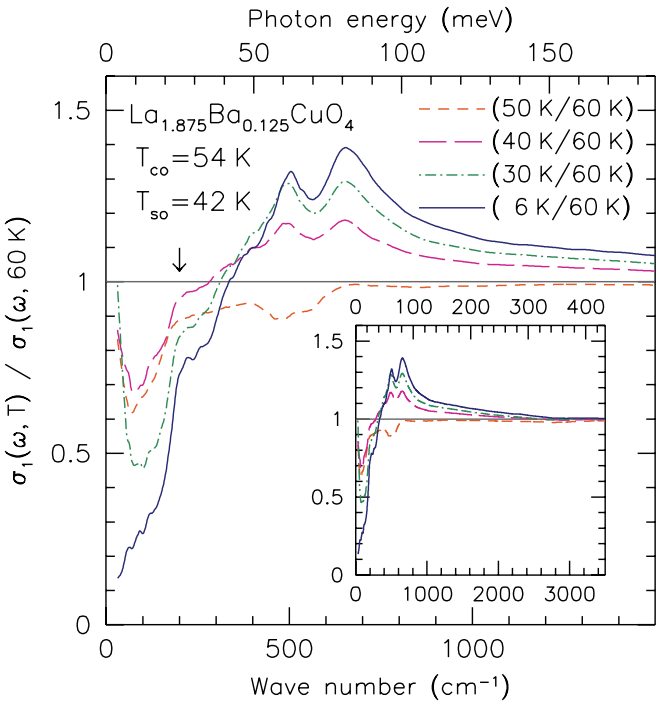

FIG. 15. (Color online) The temperature dependence of the smoothed ratio of the real part of the optical conductivity with the 60 K data. The phonons and antiresonances have been subtracted. The arrow denotes a kink attributed to the formation of a gap on the Fermi arc below T_{so}. Inset: the ratio over a wide frequency range.

long-range order for 40 K $\gtrsim T >$ 16 K. As a consequence, there should be a finite scattering rate associated with the "superconducting" features. The small but finite width of the $\omega = 0$ ("Drude") peak for 16 K $< T \lesssim$ 50 K is consistent with this expectation. The development of the finite-frequency peak is qualitatively compatible with Orenstein's prediction for a modulated superconductor, although it appears at a frequency somewhat lower than $\tilde{\omega}_{p,S}$. The shifted spectral weight appears to be pushed above $2\Delta_0$, where ARPES studies[56,57] indicate $2\Delta_0 \approx 40$ meV in the antinodal region.

There are some experimental results that complicate this picture. The ARPES studies[56,57] indicate a d-wave-like gap along the near-nodal arc for $T \lesssim 40$ K, whereas the PDW state is predicted to have a gapless near-nodal arc.[146] The d-wave-like gap suggests the presence of a more uniform superconducting component that develops below ∼40 K. Such a uniform component might be necessary to get bulk superconductivity at low temperature, as the correlation length of the PDW order is limited by that of the stripe order, which is restricted to several hundred angströms.[46,47] Of course, if a uniform component is present, then one returns to the challenge of explaining why the interlayer Josephson coupling is frustrated.

A different complication is that a substantial narrowing of the zero-frequency peak is already apparent at 50 K, where we have no enhancement at ∼80 meV. At that temperature, we have charge stripe order but not spin order, and the spin order may be necessary to pin the phase of $\rho_s(\mathbf{r})$ with respect to the lattice. Perhaps at 50 K, in the absence of pinning, the PDW correlations start to show up at low frequency but not at higher frequency. In any case, the high-frequency peak remains at 6 K, below the point where 2D superconducting order develops,[29] so that the modulated ρ_s should still be present there.

IV. CONCLUSIONS

The temperature dependence of the optical properties of $La_{2-x}Ba_xCuO_4$ for light polarized in the a-b planes and along the poorly conducting c axis has been determined for $x =$ 0.095, 0.125, and 0.145. The $x = 0.095$ and 0.145 samples are superconducting, with $T_c = 32$ and ≃24 K, respectively. The in-plane optical conductivity can be characterized as a Drude-like response that narrows with decreasing temperature, superimposed on a flat, incoherent background; below T_c missing low-frequency spectral weight is the hallmark of the formation of a superconducting condensate. Interestingly, in both cases $\omega^2_{p,S}/\omega^2_{p,D} < 1$, indicating that only a fraction of the normal-state carriers condense; this is consistent with the observation of strong dissipation in the normal state.

The optical properties along the poorly conducting c axis in the $x = 0.095$ and 0.145 materials are insulating in character, dominated by the normally infrared-active phonons with only a weak electronic background; new lattice modes appear at the HTT→LTO transition. Below T_c, a sharp plasma edge is observed in the c-axis reflectance; this feature is attributed to the formation of a supercurrent along the c axis due to Josephson coupling between the copper-oxygen planes. Despite the dramatic reduction in the c-axis resistivity below T_{so} in the 1/8 material, no Josephson plasma edge or hint of metallic behavior is observed. In the superconducting materials, the spectral weight of the condensate for the a-b plane and the c axis fall on the universal scaling line $\rho_{s0}/8 \simeq 4.4\,\sigma_{dc}\,T_c$.

The behavior of the anomalous $x = 1/8$ phase in which the superconductivity is dramatically weakened ($T_c \simeq 2.4$ K) stands out in stark contrast. The in-plane optical properties are similar to the other two dopings at high temperature; however, close to or below T_{so} there is an unusual suppression of the reflectance over much of the infrared region and a transfer of spectral weight from low frequency to energies above ≃40 meV, indicating the formation of a momentum-dependent energy gap. Below T_{so}, the free-carrier response continues to narrow dramatically with decreasing temperature, to the extent that at the lowest measured temperature the spectral weight associated with the free carriers can no longer be observed. This response mimics the missing spectral weight associated with the formation of a condensate; however, we are currently unable to distinguish a momentum-dependent CDW gap from the similar behavior expected from a PDW state.

ACKNOWLEDGMENTS

We would like to thank A. Akrap, A. Auerbach, D. N. Basov, D. A. Crandles, S. V. Dordevic, J. Hwang, S. A. Kivelson, M. Reedyk, T. Timusk, and N. L. Wang for useful discussions, and M. G. Rechner for careful reading of this manuscript. Research supported by the US Department of Energy, Office of Basic Energy Sciences, Division of Materials Sciences and Engineering under Contract No. DE-AC02-98CH10886.

*homes@bnl.gov

[1] J. G. Bednorz and K. A. Müller, Z. Phys. B **64**, 189 (1986).

[2] C. W. Chu, L. Gao, F. Chen, Z. J. Huang, R. L. Meng, and Y. Y. Xue, Nature (London) **365**, 323 (1993).

[3] *Physical Properties of High Temperature Superconductors*, edited by D. M. Ginsberg Vols. I–V (World Scientific, Singapore, 1989–1996).

[4] D. J. Van Harlingen, Rev. Mod. Phys. **67**, 515 (1995).

[5] T. Timusk and B. Statt, Rep. Prog. Phys. **62**, 61 (1999).

[6] J. Orenstein and A. J. Millis, Science **288**, 468 (2000).

[7] A. Damascelli, Z. Hussain, and Z.-X. Shen, Rev. Mod. Phys. **75**, 473 (2003).

[8] D. N. Basov and T. Timusk, Rev. Mod. Phys. **77**, 721 (2005).

[9] P. A. Lee, N. Nagaosa, and X.-G. Wen, Rev. Mod. Phys. **78**, 17 (2006).

[10] D. N. Basov, R. D. Averitt, D. van der Marel, M. Dressel, and K. Haule, Rev. Mod. Phys. **83**, 471 (2011).

[11] H. Takagi, T. Ido, S. Ishibashi, M. Uota, S. Uchida, and Y. Tokura, Phys. Rev. B **40**, 2254 (1989).

[12] M. R. Presland, J. L. Tallon, R. G. Buckley, R. S. Liu, and N. E. Flower, Physica C **176**, 95 (1991).

[13] J. L. Tallon, C. Bernhard, H. Shaked, R. L. Hitterman, and J. D. Jorgensen, Phys. Rev. B **51**, 12911 (1995).

[14] D. M. Broun, Nat. Phys. **4**, 170 (2008).

[15] A. R. Moodenbaugh, Y. Xu, M. Suenaga, T. J. Folkerts, and R. N. Shelton, Phys. Rev. B **38**, 4596 (1988).

[16] N. Yamada and M. Ido, Physica C **203**, 240 (1992).

[17] M. Akoshima, T. Noji, Y. Ono, and Y. Koike, Phys. Rev. B **57**, 7491 (1998).

[18] R. Liang, D. A. Bonn, and W. N. Hardy, Phys. Rev. B **73**, 180505(R) (2006).

[19] J. D. Axe, A. H. Moudden, D. Hohlwein, D. E. Cox, K. M. Mohanty, A. R. Moodenbaugh, and Y. Xu, Phys. Rev. Lett. **62**, 2751 (1989).

[20] K. Kumagai, H. Matoba, N. Wada, M. Okaji, and K. Nara, J. Phys. Soc. Jpn. **60**, 1448 (1991).

[21] S. J. L. Billinge, G. H. Kwei, A. C. Lawson, J. D. Thompson, and H. Takagi, Phys. Rev. Lett. **71**, 1903 (1993).

[22] S. Katano, J. A. Fernandez-Baca, S. Funahashi, N. Môri, Y. Ueda, and K. Koga, Physica C **214**, 64 (1993).

[23] G. M. Luke, L. P. Le, B. J. Sternlieb, W. D. Wu, Y. J. Uemura, J. H. Brewer, T. M. Riseman, S. Ishibashi, and S. Uchida, Physica C **185–189**, 1175 (1991).

[24] G. Luke, K. Kojima, M. Larkin, J. Merrin, B. Nachumi, Y. Uemura, Y. Nakamura, S. Uchida, and M. Crawford, Hyperfine Interact. **105**, 113 (1997).

[25] J. Arai, T. Ishiguro, T. Goko, S. Iigaya, K. Nishiyama, I. Watanabe, and K. Nagamine, J. Low Temp. Phys. **131**, 375 (2003).

[26] C. C. Homes, S. V. Dordevic, G. D. Gu, Q. Li, T. Valla, and J. M. Tranquada, Phys. Rev. Lett. **96**, 257002 (2006).

[27] G. Xu, J. M. Tranquada, T. G. Perring, G. D. Gu, M. Fujita, and K. Yamada, Phys. Rev. B **76**, 014508 (2007).

[28] Q. Li, M. Hücker, G. D. Gu, A. M. Tsvelik, and J. M. Tranquada, Phys. Rev. Lett. **99**, 067001 (2007).

[29] J. M. Tranquada, G. D. Gu, M. Hücker, Q. Jie, H.-J. Kang, R. Klingeler, Q. Li, N. Tristan, J. S. Wen, G. Y. Xu, Z. J. Xu, J. Zhou, and M. v. Zimmermann, Phys. Rev. B **78**, 174529 (2008).

[30] J. Wen, Z. Xu, G. Xu, J. M. Tranquada, G. Gu, S. Chang, and H. J. Kang, Phys. Rev. B **78**, 212506 (2008).

[31] J. Kim, A. Kagedan, G. D. Gu, C. S. Nelson, and Y.-J. Kim, Phys. Rev. B **77**, 180513 (2008).

[32] J. Kim, H. Zhang, G. D. Gu, and Y.-J. Kim, J. Supercond. Novel Magn. **22**, 251 (2009).

[33] S. Wakimoto, H. Kimura, K. Ishii, K. Ikeuchi, T. Adachi, M. Fujita, K. Kakurai, Y. Koike, J. Mizuki, Y. Noda, K. Yamada, A. H. Said, and Y. Shvyd'ko, Phys. Rev. Lett. **102**, 157001 (2009).

[34] J. Wen, Q. Jie, Q. Li, M. Hücker, M. v. Zimmermann, S. J. Han, Z. Xu, D. K. Singh, L. Zhang, G. Gu, and J. M. Tranquada, e-print arXiv:1009.0031.

[35] T. Adachi, N. Kitajima, and Y. Koike, Phys. Rev. B **83**, 060506 (2011).

[36] M. Fujita, H. Goka, K. Yamada, J. M. Tranquada, and L. P. Regnault, Phys. Rev. B **70**, 104517 (2004).

[37] J. M. Tranquada, H. Woo, T. G. Perring, H. Goka, G. D. Gu, G. Xu, M. Fujita, and K. Yamada, Nature (London) **429**, 534 (2004).

[38] P. Abbamonte, A. Rusydi, S. Smadici, G. D. Gu, G. A. Sawatzky, and D. L. Feng, Nat. Phys. **1**, 155 (2005).

[39] D. Reznik, L. Pintschovius, M. Ito, S. Iikubo, M. Sato, H. Goka, M. Fujita, K. Yamada, J. M. Gu, and G. D. Tranquada, Nature (London) **440**, 1170 (2006).

[40] Y. Zhao, B. D. Gaulin, J. P. Castellan, J. P. C. Ruff, S. R. Dunsiger, G. D. Gu, and H. A. Dabkowska, Phys. Rev. B **76**, 184121 (2007).

[41] S. R. Dunsiger, Y. Zhao, Z. Yamani, W. J. L. Buyers, H. A. Dabkowska, and B. D. Gaulin, Phys. Rev. B **77**, 224410 (2008).

[42] S. R. Dunsiger, Y. Zhao, B. D. Gaulin, Y. Qiu, P. Bourges, Y. Sidis, J. R. D. Copley, A. Kallin, E. M. Mazurek, and H. A. Dabkowska, Phys. Rev. B **78**, 092507 (2008).

[43] M. v. Zimmermann, R. Nowak, G. D. Gu, C. Mennerich, H.-H. Klauss, and M. Hücker, Rev. Sci. Instrum. **79**, 033906 (2008).

[44] M. Hücker, G. D. Gu, and J. M. Tranquada, Phys. Rev. B **78**, 214507 (2008).

[45] M. Hücker, M. v. Zimmermann, M. Debessai, J. S. Schilling, J. M. Tranquada, and G. D. Gu, Phys. Rev. Lett. **104**, 057004 (2010).

[46] M. Hücker, M. v. Zimmermann, G. D. Gu, Z. J. Xu, J. S. Wen, G. Xu, H. J. Kang, A. Zheludev, and J. M. Tranquada, Phys. Rev. B **83**, 104506 (2011).

[47] S. B. Wilkins, M. P. M. Dean, J. Fink, M. Hücker, J. Geck, V. Soltwisch, E. Schierle, E. Weschke, G. Gu, S. Uchida, N. Ichikawa, J. M. Tranquada, and J. P. Hill, Phys. Rev. B **84**, 195101 (2011).

[48] J. Zaanen and O. Gunnarsson, Phys. Rev. B **40**, 7391 (1989).

[49] J. M. Tranquada, B. J. Sternlieb, J. D. Axe, Y. Nakamura, and S. Uchida, Nature (London) **375**, 561 (1995).

[50] S. A. Kivelson, I. P. Bindloss, E. Fradkin, V. Oganesyan, J. M. Tranquada, A. Kapitulnik, and C. Howald, Rev. Mod. Phys. **75**, 1201 (2003).

[51] M. Vojta and S. Sachdev, Phys. Rev. Lett. **83**, 3916 (1999).

[52] M. Vojta, Adv. Phys. **58**, 699 (2009).

[53] T. Ekino, A. M. Gabovich, M. S. Li, M. Pekała, H. Szymczak, and A. I. Voitenko, J. Phys.: Condens. Matter **23**, 385701 (2011).

[54] E. Berg, E. Fradkin, E.-A. Kim, S. A. Kivelson, V. Oganesyan, J. M. Tranquada, and S. C. Zhang, Phys. Rev. Lett. **99**, 127003 (2007).

[55] J. F. Ding, X. Q. Xiang, Y. Q. Zhang, H. Liu, and X. G. Li, Phys. Rev. B **77**, 214524 (2008).

[56] T. Valla, A. V. Fedorov, J. Lee, J. C. Davis, and G. D. Gu, Science **314**, 1914 (2006).

[57] R.-H. He, K. Tanaka, S.-K. Mo, T. Sasagawa, M. Fujita, T. Adachi, N. Mannella, K. Yamada, Y. Koike, Z. Hussain, and Z.-X. Shen, Nat. Phys. **5**, 119 (2009).

[58] A. Kanigel, M. R. Norman, M. Randeria, U. Chatterjee, S. Souma, A. Kaminski, H. M. Fretwell, S. Rosenkranz, M. Shi, T. Sato, T. Takahashi, Z. Z. Li, H. Raffy, K. Kadowaki, D. Hinks, L. Ozyuzer, and J. C. Campuzano, Nat. Phys. **2**, 447 (2006).

[59] T. Kondo, T. Takeuchi, A. Kaminski, S. Tsuda, and S. Shin, Phys. Rev. Lett. **98**, 267004 (2007).

[60] S. Hüfner, M. A. Hossain, A. Damascelli, and G. A. Sawatzky, Rep. Prog. Phys. **71**, 062501 (2008).

[61] S. Tajima, N. L. Wang, N. Ichikawa, H. Eisaki, S. Uchida, H. Kitano, T. Hanaguri, and A. Maeda, Europhys. Lett. **47**, 715 (1999).

[62] S. Tajima, T. Noda, H. Eisaki, and S. Uchida, Phys. Rev. Lett. **86**, 500 (2001).

[63] M. Dumm, D. N. Basov, S. Komiya, Y. Abe, and Y. Ando, Phys. Rev. Lett. **88**, 147003 (2002).

[64] A. Lucarelli, S. Lupi, M. Ortolani, P. Calvani, P. Maselli, M. Capizzi, P. Giura, H. Eisaki, N. Kikugawa, T. Fujita, M. Fujita, and K. Yamada, Phys. Rev. Lett. **90**, 037002 (2003).

[65] W. J. Padilla, M. Dumm, S. Komiya, Y. Ando, and D. N. Basov, Phys. Rev. B **72**, 205101 (2005).

[66] A. Lucarelli, S. Lupi, M. Ortolani, P. Calvani, P. Maselli, and M. Capizzi, Phys. Rev. Lett. **91**, 129702 (2003).

[67] S. Tajima, S. Uchida, D. van der Marel, and D. N. Basov, Phys. Rev. Lett. **91**, 129701 (2003).

[68] M. Tinkham, *Introduction to Superconductivity* (McGraw-Hill, New York, 1966).

[69] A. A. Schafgans, C. C. Homes, G. D. Gu, S. Komiya, Y. Ando, and D. N. Basov, Phys. Rev. B **82**, 100505(R) (2010).

[70] C. C. Homes, S. V. Dordevic, M. Strongin, D. A. Bonn, R. Liang, W. N. Hardy, S. Komiya, Y. Ando, G. Yu, N. Kaneko, X. Zhao, M. Greven, D. N. Basov, and T. Timusk, Nature (London) **430**, 539 (2004).

[71] C. C. Homes, S. V. Dordevic, T. Valla, and M. Strongin, Phys. Rev. B **72**, 134517 (2005).

[72] C. C. Homes, S. V. Dordevic, D. A. Bonn, R. Liang, W. N. Hardy, and T. Timusk, Phys. Rev. B **71**, 184515 (2005).

[73] C. C. Homes, Phys. Rev. B **80**, 180509(R) (2009).

[74] S. Barišić and J. Zelenko, Solid State Commun. **74**, 367 (1990).

[75] J. Wen, Z. Xu, G. Xu, Q. Jie, M. Hücker, A. Zheludev, W. Tian, B. L. Winn, J. L. Zarestky, D. K. Singh, T. Hong, Q. Li, G. Gu, and J. M. Tranquada, e-print arXiv:1111.5383.

[76] V. L. Berezinskii, Zh. Eksp. Teor. Fiz. **61**, 1144 (1971) [Sov. Phys. JETP **34**, 610 (1972)].

[77] J. M. Kosterlitz and D. J. Thouless, J. Phys. C **6**, 1181 (1973).

[78] C. C. Homes, M. Reedyk, D. A. Crandles, and T. Timusk, Appl. Opt. **32**, 2976 (1993).

[79] C. C. Homes, G. L. Carr, R. P. S. M. Lobo, J. D. LaVeigne, and D. B. Tanner, Appl. Opt. **46**, 7884 (2007).

[80] M. Reedyk and T. Timusk, Phys. Rev. Lett. **69**, 2705 (1992).

[81] J. H. Kim, B. J. Feenstra, H. S. Somal, D. van der Marel, W. Y. Lee, A. M. Gerrits, and A. Wittlin, Phys. Rev. B **49**, 13065 (1994).

[82] T. Startseva, T. Timusk, M. Okuya, T. Kimura, and K. Kishio, Physica C **321**, 135 (1999).

[83] A. A. Tsvetkov, D. Dulić, D. van der Marel, A. Damascelli, G. A. Kaljushnaia, J. I. Gorina, N. N. Senturina, N. N. Kolesnikov, Z. F. Ren, J. H. Wang, A. A. Menovsky, and T. T. M. Palstra, Phys. Rev. B **60**, 13196 (1999).

[84] S. Tajima, Y. Fudamoto, T. Kakeshita, B. Gorshunov, V. Železný, K. M. Kojima, M. Dressel, and S. Uchida, Phys. Rev. B **71**, 094508 (2005).

[85] C. C. Homes, J. M. Tranquada, and D. J. Buttrey, Phys. Rev. B **75**, 045128 (2007).

[86] M. Dressel and G. Grüner, *Electrodynamics of Solids* (Cambridge University Press, Cambridge, 2001).

[87] F. Wooten, in *Optical Properties of Solids* (Academic Press, New York, 1972), pp. 244–250.

[88] C. C. Homes, A. W. McConnell, B. P. Clayman, D. A. Bonn, R. Liang, W. N. Hardy, M. Inoue, H. Negishi, P. Fournier, and R. L. Greene, Phys. Rev. Lett. **84**, 5391 (2000).

[89] D. Y. Smith, in *Handbook of Optical Constants of Solids*, edited by E. D. Palik (Academic, New York, 1985), pp. 35–68.

[90] To allow for the data to be fit over the entire frequency range, two high-frequency oscillators have also been included at $\simeq$13 000 and 21 000 cm^{-1}.

[91] R. A. Ferrell and R. E. Glover III, Phys. Rev. **109**, 1398 (1958).

[92] M. Tinkham and R. A. Ferrell, Phys. Rev. Lett. **2**, 331 (1959).

[93] C. Jiang, E. Schachinger, J. P. Carbotte, D. Basov, and T. Timusk, Phys. Rev. B **54**, 1264 (1996).

[94] C. C. Homes, J. M. Tranquada, Q. Li, A. R. Moodenbaugh, and D. J. Buttrey, Phys. Rev. B **67**, 184516 (2003).

[95] Y. Ando, A. N. Lavrov, S. Komiya, K. Segawa, and X. F. Sun, Phys. Rev. Lett. **87**, 017001 (2001).

[96] M. Sutherland, D. G. Hawthorn, R. W. Hill, F. Ronning, S. Wakimoto, H. Zhang, C. Proust, E. Boaknin, C. Lupien, L. Taillefer, R. Liang, D. A. Bonn, W. N. Hardy, R. Gagnon, N. E. Hussey, T. Kimura, M. Nohara, and H. Takagi, Phys. Rev. B **67**, 174520 (2003).

[97] Y. S. Lee, K. Segawa, Z. Q. Li, W. J. Padilla, M. Dumm, S. V. Dordevic, C. C. Homes, Y. Ando, and D. N. Basov, Phys. Rev. B **72**, 054529 (2005).

[98] M. M. Qazilbash, J. J. Hamlin, R. E. Baumbach, L. Zhang, D. J. Singh, M. B. Maple, and D. N. Basov, Nat. Phys. **5**, 647 (2009).

[99] J. W. Allen and J. C. Mikkelsen, Phys. Rev. B **15**, 2952 (1977).

[100] A. V. Puchkov, D. N. Basov, and T. Timusk, J. Phys.: Condens. Matter **8**, 10049 (1996).

[101] E. Schachinger, C. C. Homes, R. P. S. M. Lobo, and J. P. Carbotte, Phys. Rev. B **78**, 134522 (2008).

[102] E. Schachinger, J. J. Tu, and J. P. Carbotte, Phys. Rev. B **67**, 214508 (2003).

[103] S. V. Dordevic, C. C. Homes, J. J. Tu, T. Valla, M. Strongin, P. D. Johnson, G. D. Gu, and D. N. Basov, Phys. Rev. B **71**, 104529 (2005).

[104] J. Hwang, T. Timusk, E. Schachinger, and J. P. Carbotte, Phys. Rev. B **75**, 144508 (2007).

[105] J. Hwang, T. Timusk, and G. D. Gu, J. Phys.: Condens. Matter **19**, 125208 (2007).

[106] J. Hwang, E. Schachinger, J. P. Carbotte, F. Gao, D. B. Tanner, and T. Timusk, Phys. Rev. Lett. **100**, 137005 (2008).

[107] H. He, Y. Sidis, P. Bourges, G. D. Gu, A. Ivanov, N. Koshizuka, B. Liang, C. T. Lin, L. P. Regnault, E. Schoenherr, and B. Keimer, Phys. Rev. Lett. **86**, 1610 (2001).

[108] H. He, P. Bourges, Y. Sidis, C. Ulrich, L. P. Regnault, S. Pailhs, N. S. Berzigiarova, N. N. Kolesnikov, and B. Keimer, Science **295**, 1045 (2002).

[109]J. Yang, J. Hwang, E. Schachinger, J. P. Carbotte, R. P. S. M. Lobo, D. Colson, A. Forget, and T. Timusk, Phys. Rev. Lett. **102**, 027003 (2009).
[110]J. Hwang, J. P. Carbotte, and T. Timusk, Phys. Rev. Lett. **100**, 177005 (2008).
[111]J. Chang, A. P. Schnyder, R. Gilardi, H. M. Rønnow, S. Pailhes, N. B. Christensen, C. Niedermayer, D. F. McMorrow, A. Hiess, A. Stunault, M. Enderle, B. Lake, O. Sobolev, N. Momono, M. Oda, M. Ido, C. Mudry, and J. Mesot, Phys. Rev. Lett. **98**, 077004 (2007).
[112]J. Chang, C. Niedermayer, R. Gilardi, N. B. Christensen, H. M. Rønnow, D. F. McMorrow, M. Ay, J. Stahn, O. Sobolev, A. Hiess, S. Pailhes, C. Baines, N. Momono, M. Oda, M. Ido, and J. Mesot, Phys. Rev. B **78**, 104525 (2008).
[113]Y. J. Uemura, G. M. Luke, B. J. Sternlieb, J. H. Brewer, J. F. Carolan, W. N. Hardy, R. Kadono, J. R. Kempton, R. F. Kiefl, S. R. Kreitzman, P. Mulhern, T. M. Riseman, D. L. Williams, B. X. Yang, S. Uchida, H. Takagi, J. Gopalakrishnan, A. W. Sleight, M. A. Subramanian, C. L. Chien, M. Z. Cieplak, G. Xiao, V. Y. Lee, B. W. Statt, C. E. Stronach, W. J. Kossler, and X. H. Yu, Phys. Rev. Lett. **62**, 2317 (1989).
[114]J. Zaanen, Nature (London) **430**, 512 (2004).
[115]J. L. Tallon, J. R. Cooper, S. H. Naqib, and J. W. Loram, Phys. Rev. B **73**, 180504 (2006).
[116]N. H. Lindner and A. Auerbach, Phys. Rev. B **81**, 054512 (2010).
[117]D. N. Basov and A. V. Chubukov, Nat. Phys. **7**, 272 (2011).
[118]K. Tamasaku, Y. Nakamura, and S. Uchida, Phys. Rev. Lett. **69**, 1455 (1992).
[119]C. C. Homes, T. Timusk, R. Liang, D. A. Bonn, and W. N. Hardy, Phys. Rev. Lett. **71**, 1645 (1993).
[120]C. C. Homes, T. Timusk, D. A. Bonn, R. Liang, and W. N. Hardy, Physica C **254**, 265 (1995).
[121]S. Uchida, K. Tamasaku, and S. Tajima, Phys. Rev. B **53**, 14558 (1996).
[122]S. Tajima, J. Schützmann, S. Miyamoto, I. Terasaki, Y. Sato, and R. Hauff, Phys. Rev. B **55**, 6051 (1997).
[123]D. Dulić, D. van der Marel, A. A. Tsvetkov, W. N. Hardy, Z. F. Ren, J. H. Wang, and B. A. Willemsen, Phys. Rev. B **60**, R15051 (1999).
[124]T. Motohashi, J. Shimoyama, K. Kitazawa, K. Kishio, K. M. Kojima, S. Uchida, and S. Tajima, Phys. Rev. B **61**, R9269 (2000).
[125]S. V. Dordevic, S. Komiya, Y. Ando, and D. N. Basov, Phys. Rev. Lett. **91**, 167401 (2003).
[126]S. V. Dordevic, S. Komiya, Y. Ando, Y. J. Wang, and D. N. Basov, Phys. Rev. B **71**, 054503 (2005).
[127]T. Shibauchi, H. Kitano, K. Uchinokura, A. Maeda, T. Kimura, and K. Kishio, Phys. Rev. Lett. **72**, 2263 (1994).
[128]D. N. Basov, T. Timusk, B. Dabrowski, and J. D. Jorgensen, Phys. Rev. B **50**, 3511 (1994).
[129]R. J. Radtke and K. Levin, Physica C **250**, 282 (1995).
[130]D. N. Basov, R. Liang, B. Dabrowski, D. A. Bonn, W. N. Hardy, and T. Timusk, Phys. Rev. Lett. **77**, 4090 (1996).
[131]M. Prohammer and J. P. Carbotte, Phys. Rev. B **43**, 5370 (1991).
[132]K. Zhang, D. A. Bonn, S. Kamal, R. Liang, D. J. Baar, W. N. Hardy, D. Basov, and T. Timusk, Phys. Rev. Lett. **73**, 2484 (1994).
[133]S. Chakravarty, A. Sudbø, P. W. Anderson, and S. Strong, Science **261**, 337 (1993).
[134]T. Xiang and J. M. Wheatley, Phys. Rev. Lett. **77**, 4632 (1996).
[135]L. B. Ioffe and A. J. Millis, Science **285**, 1241 (1999).
[136]A. Hosseini, S. Kamal, D. A. Bonn, R. Liang, and W. N. Hardy, Phys. Rev. Lett. **81**, 1298 (1998).
[137]H. F. Hess, R. B. Robinson, R. C. Dynes, J. M. Valles, and J. V. Waszczak, J. Vac. Sci. Technol. A **8**, 450 (1990).
[138]C. Wang, B. Giambattista, C. G. Slough, R. V. Coleman, and M. A. Subramanian, Phys. Rev. B **42**, 8890 (1990).
[139]A. W. McConnell, B. P. Clayman, C. C. Homes, M. Inoue, and H. Negishi, Phys. Rev. B **58**, 13565 (1998).
[140]S. V. Dordevic, D. N. Basov, R. C. Dynes, and E. Bucher, Phys. Rev. B **64**, 161103(R) (2001).
[141]G. Grüner, *Density Waves in Solids* (Addison-Wesley, Reading, MA, 1994).
[142]A. Himeda, T. Kato, and M. Ogata, Phys. Rev. Lett. **88**, 117001 (2002).
[143]E. Berg, E. Fradkin, S. A. Kivelson, and J. M. Tranquada, New J. Phys. **11**, 115004 (2009).
[144]S. Barabash, D. Stroud, and I.-J. Hwang, Phys. Rev. B **61**, R14924 (2000).
[145]J. Orenstein, Physica C **390**, 243 (2003).
[146]S. Baruch and D. Orgad, Phys. Rev. B **77**, 174502 (2008).